PREDICTION OF ICE ACCRETION AND CFD ANALYSIS OF NACA 2412 AIRFOIL FOR EVALUATION OF AERODYNAMIC PERFORMANCE DEGRADATION

MAHBUBA FERDOUS

MILITARY INSTITUTE OF SCIENCE AND TECHNOLOGY

2019

PREDICTION OF ICE ACCRETION AND CFD ANALYSIS OF NACA 2412 AIRFOIL FOR EVALUATION OF AERODYNAMIC PERFORMANCE DEGRADATION

MAHBUBA FERDOUS

(B.Sc Engg., MIST)

A THESIS SUBMITTED

FOR THE DEGREE OF MASTER OF SCIENCE

DEPARTMENT OF AERONAUTICAL ENGINEERING

MILITARY INSTITUTE OF SCIENCE AND TECHNOLOGY

2019

PREDICTION OF ICE ACCRETION AND CFD ANALYSIS OF NACA 2412 AIRFOIL FOR EVALUATION OF AERODYNAMIC PERFORMANCE DEGRADATION

A Thesis Submitted to the Department of Aeronautical Engineering, Military Institute of Science and Technology (MIST) in Partial Fulfillment of the Requirement for the Degree of Master of Science in Aeronautical Engineering

MAHBUBA FERDOUS

(B.Sc Engg., MIST)

Department of Aeronautical Engineering

Military Institute of Science and Technology (MIST)

Dhaka, Bangladesh

August, 2019

The thesis titled "**PREDICTION OF ICE ACCRETION AND CFD ANALYSIS OF NACA 2412 AIRFOIL FOR EVALUATION OF AERODYNAMIC PERFORMANCE DEGRADATION**" submitted by **Mahbuba Ferdous;** Roll No: **1016220007 (P);** Session: April, 2016 has been accepted as satisfactory in partial fulfillment of the requirement for the degree of Master of Science in Aeronautical Engineering on ……. August, 2019.

BOARD OF EXAMINERS

1.	…….. Associate Professor Wg Cdr Vikram Deshpande, PhD Department of Aeronautical Engineering MIST, Dhaka- 1216, Bangladesh	**Chairman (Supervisor)**
2.	……. Air Cdre Md Abdus Salam, BPP, psc Head, Department of Aeronautical Engineering MIST, Dhaka- 1216, Bangladesh	**Member (Ex- Officio)**
3.	…… Professor Dr. M A Taher Ali Department of Aeronautical Engineering MIST, Dhaka- 1216, Bangladesh	**Member (Internal)**
4.	…… Professor Dr. Md. Quamrul Islam Department of Mechanical Engineering MIST, Dhaka- 1216, Bangladesh	**Member (Internal)**
5.	…… Professor Dr. Maglub Al Nur Department of Mechanical Engineering BUET, Dhaka- 1000, Bangladesh	**Member (External)**

DECLARATION

I do hereby declare that this thesis is my original work and I have written it in its entirety. I have duly acknowledged all the sources of information which have been used in the thesis. This thesis has not also been submitted for any degree in any university previously.

……

Mahbuba Ferdous

August 2019

ACKNOWLEDGEMENT

At the very outset, the author expresses her deepest gratitude and profound indebtedness to her supervisor, Associate Professor Wg Cdr Vikram Deshpande, PhD, Department of Aeronautical Engineering, MIST, Dhaka for his continuous guidance, valuable suggestions and encouragement to the research work all through the time. His relentless support and advice at every stage made this research work possible and fruitful one.

The author is also thankful to Air Cdre Md. Abdus Salam, BPP, psc, Head, Department of Aeronautical Engineering, MIST for the support and guidance he has provided. Finally the author would also like to express her sincere gratitude to Prof Dr. M A Taher Ali, Department of Aeronautical Engineering, MIST for his valuable guidance and thanks to all members of the Department of Aeronautical Engineering, MIST for their cooperation for successful completion of the work.

TABLE OF CONTENTS

ABSTRACT

High altitude flights possess significant icing hazard in certain type of atmospheric conditions. This ice accretion on aircraft wing leading edges and engine nacelle pose threat to the flight safety. From early days of beginning of high altitude flights, numerous studies have been undertaken to determine the effects of icing on aircraft performance. Bangladesh is now moving at galloping pace in the aviation industry, and is expected to take leap of high altitude flight designs in near term period. This could be accomplished if several technologies are developed in-house prior to design and development of high altitude flights. One such requirement is the development of code for prediction of ice accretion and subsequently to design the anti-icing system.

With this long term goal in mind, the present research focuses on understanding of the analytical approaches to predict ice accretion physics on aircraft wing cross section. Using the existing ice accretion thermodynamic and other conservation laws presented in open literature, a computer code was developed to predict the ice accretion over the airfoil. The code developed was validated against the experimental ice shapes from the open literatures. Using the developed code, the ice accretion prediction is undertaken on a specific airfoil i.e. NACA 2412, a most common airfoil cross section for moderately high altitude flights.

The aerodynamic performance of the predicted ice accretion was analyzed using the Computational Fluid Dynamic (CFD) technique. The aerodynamic study was undertaken for three different icing conditions and it suggests that the ice accreted airfoil possesses lower lift than the base airfoil. It is also observed that the increase in the drag for ice accreted airfoil is significant as compared to base airfoil. Results of the study show that, most critical and worst icing occurs in presence of altocumulus clouds forming mixed ice on the airfoil leading edges. Such icing conditions result in reduction in lift coefficient and increase in drag coefficient approximately by 90% and 800% respectively compared to the base airfoil. These observations are in consonance with the published literature available in open domain.

The current research is considered as the stepping stone for subsequent development and improvement of icing codes as well as design of anti-icing systems.

LIST OF FIGURES

LIST OF TABLES

NOMENCLATURE

c : Chord length, m

β : Collection efficiency, dimensionless

f :Freezing fraction, dimensionless

h : Ice thickness, m

LWC : Liquid Water Content, Kg/m^3

$\dot{m}$: Mass flow rate, Kg/s

$\dot{e}$: Energy flow rate, J/s

ρ : Density, Kg/m^3

T : Temperature, K

S : Surface length, m

t :Icing time, sec

V : Free- stream velocity, m/s

MVD : Median Volume Diameter, m

R_e : Reynolds number, dimensionless

SLD :Super Cooled Droplets

µ : Viscosity of air, Kg/ms

AoA : Angle of attack (Deg)

h_c : Convective heat transfer coefficient, W/m^2 K

Nu : Nusselt Number, dimensionless

K : Thermal conductivity, W/mK

P : Static pressure, N/ m^2

C_p : Specific heat, J/kg/K

L_f : Latent heat of fusion, J/kg

L_v : Latent heat of vaporization, J/kg

Subscripts

com : Impinging water

conv : Convection

a : Air

i : Ice

ice : Freezing ice

w : Liquid Water

in : Runback into the control volume

out : Runback out of control volume

sur : Surface condition

eva :Evaporation

I : Control volume

I-1 : Preceding control volume

CHAPTER 1
INTRODUCTION

1.1 Overview

With the widespread use of aircraft in various sectors such as commercial, aerobatic and private flights, exploration and rescue operation, it is the demand of time that aircraft should be able to fly in difficult situations and adverse weather condition. As the aircraft has to operate the over long distance and at medium to higher altitude (10,000 ft to 25,000 ft), it is often affected with various meteorological factors like rainfall, super-cooled droplet impingement, liquid water content in the atmosphere etc. resulting in in-flight ice accretion. To get rid of such difficulties modern aircrafts are now equipped with ant-icing and de-icing devices. And the efficient design of such devices requires the estimation of ice and aerodynamic penalties due to icing. Thus the present research work aims at providing an input for the design of efficient anti-icing and de-icing devices for high altitude flights. This chapter thus, specifies the objectives and relevance of the study in the context of Bangladesh.

1.2 Preface

Ice accretion, in general, is deposit or coatings of ice on an object caused by the impingement and freezing of liquid (especially super cooled) water droplets present in the air. Ice build-up on air frame surface disrupts the airflow thereby increasing drag and decreasing the aircraft's ability to generate lift. Aircraft performance degradation due to large droplet ice accretion is a severe problem faced by the aviation industry from the very early days of high altitude flights. The present research work thus considers prediction of ice accretion over a NACA 2412 airfoil by using mathematical models and undertaking the Computational Fluid Dynamic analysis to assess the effects of ice accretion on the airfoil aerodynamic performance.

1.3 In- flight Icing

Icing on airplanes occurs while flying through clouds at or below zero temperatures. Aircraft can accrete ice on its aerodynamic surfaces when flying through clouds of super cooled water droplets. When these droplets impact the surface of the airfoil (usually near the leading-edge stagnation region), they will either freeze on contact or run downstream in liquid state. Depending on the surface temperature of the airfoil, this flow will either

freeze as it runs back or may simply run off the airfoil entirely. Fig. 1.1 shows an accumulation of ice on a wing leading edge.

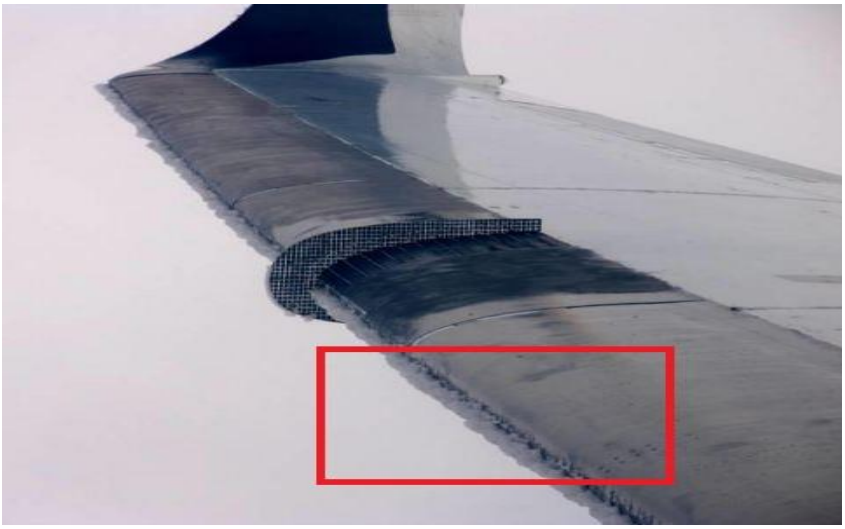

Fig. 1.1 In-flight icing on an aircraft wing [1]

From the very early years of high altitude flights aircraft icing has been recognized as one of the most significant aviation hazards. Icing can increase aerodynamic drag, weight and a reduction in lift and thrust if ice is accreted on propeller blades. All these factors may lead to a reduction in stall angle of attack and a severe degradation to overall aircraft performance. To encounter with icing problems, the angle of attack is generally increased. But icing phenomena can be extended to the exposed and unprotected areas of the aircraft. If this ice accretion process is prolonged, the aircraft will fail to maintain its stable flight causing hazardous accidents.

1.3.1 Types of in-flight icing

The severity of in- flight icing is dependent on the types of ice accumulated on different portions of the aircraft. With respect to the rate and amount of ice accretion on the surface of aircraft in-flight icing is categorized into three major types [2] which are discussed below:

- **Clear ice**

  Clear ice also known as glaze ice is a heavy coating of glassy transparent ice that is formed when aircraft is flying in areas having high concentration of large super cooled water droplets, such as cumuliform clouds and freezing rain as shown in fig 1.2. When clear ice is formed it is generally spread unevenly over the unprotected wing and tail surfaces, propeller blades, antennas, etc. It is formed when only a small part of the super cooled water droplet freezes on impact. The specific latent heat of

freezing of the water droplets released heat during freezing which raises the surface temperature to 0°C. A large portion of the water droplets is left to spread out, unite with other droplets finally freeze. Thus a solid sheet of clear and transparent ice is formed with no embedded air bubbles to weaken its structure. As the icing time is prolonged, more ice accumulates and builds up into a single or double horn shape that projects over the surface on which it is accumulating. This unique ice formation severely disrupts the airflow and is responsible for an increase in drag that may be as much as 300 to 500%.

Fig. 1.2 Side view of a wing with clear ice or glaze ice [3]

The aerodynamic effects associated with clear ice or glaze ice are:

(1) The loss of lift, because of the altered wing camber and the disruption of the smooth flow of air over the wing and tail surfaces.

(2) The increase in drag on account of the uneven and enlarged profile area of the wings.

(3) The weight of the large mass of ice which may accumulate in a short time.

(4) The vibration caused by the unequal loading on the wings and on the blades of the propeller. When large blocks break off, the vibration may become severe enough to seriously impair the structure of the airplane.

- **Rime ice**

Rime ice is an opaque, or milky white, deposit of ice that is formed when the airplane is flying through filmy/stratus type of clouds. It is dependent on a low rate of catch of small super cooled water droplets. It accumulates on the leading edges of wings and on antennas, pitot heads, etc. Rime ice is formed when the aircraft surface temperature is at a temperature below 0°C. The droplets will then freeze completely and quickly

without spreading from the point of impact. Thus, the droplets retain their spherical shape as they freeze, creating air bubbles between the frozen particles as can be seen from fig. 1.3. This process creates an irregular shape of ice [3]. Thus rime is brittle and easier to dislodge by de- icing devices compared to glaze ice.

Fig. 1.3 Side view of a wing with rime ice [3]

Because of the presence of air bubbles in between the ice structure, rime ice has a lesser weight but its danger lies in the aerodynamic alteration of the wing camber and in the choking of the instruments.

- **Mixed ice**

Mixed ice has the properties of both glaze ice and rime ice. It is formed when air is concentrated with both small and large super cooled water droplets. It appears as whitish, irregular and rough ice shapes.

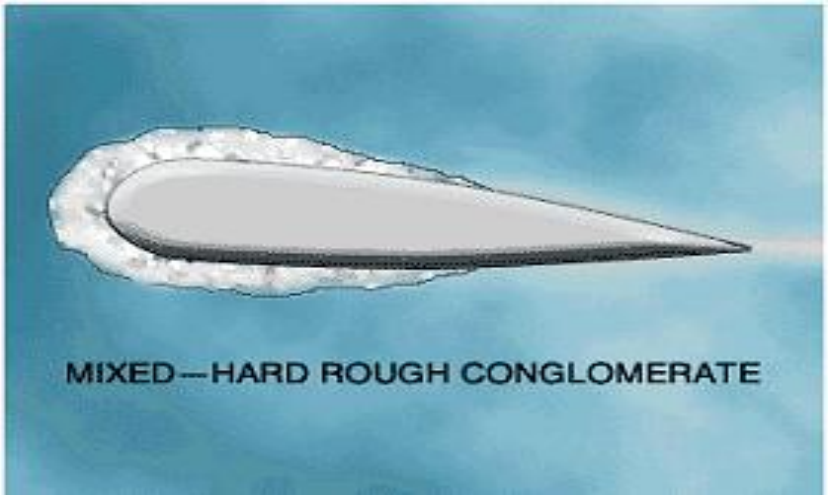

Fig. 1.4 Side view of a wing with mixed ice [3]

It is formed when the aircraft is flying in the colder portion of cumulus cloud embedded with stratus cloud and in the wet snow flakes. After the initial impact, the

remaining particles freeze rapidly and form a strong irregular shape on the leading edges of a wing or tail surfaces as seen in fig. 1.4. Ice particles are embedded in a clear ice and form a hard and rough–edged mass. As mixed ice can be formed instantly on impact and is difficult to remove by de- icing devices thereby increasingly changes aircraft flight characteristics.

1.3.2 Factors affecting aircraft icing

For an icing event to take place some form of water must be present in the atmosphere. The most essential sources are those of cloud droplets, i.e. fog, super cooled raindrops and snow particles. The mass rate of ice accreted on a structure is affected by the following factors [4].

- **Shape of aircraft surface**

The rate of ice accumulation is entirely dependent on the structural shape of the aircraft surface.The major aircraft geometrical parameters are the airfoil shape, wing leading edge radius and symmetry of the airfoil. The rate of ice accumulation is inversely proportional to the wing size and geometry. So thick wings tend to catch fewer droplets than thin wings. This is why an aircraft with thin wings flying at a high speed through large droplets has the greatest rate of icing. Surface of an aircraft that have tiny leading edges – like antennas, horizontal stabilizers, engine propeller blade, landing gear struts and rudder are the first to accumulate ice.

- **Collection efficiency, β**

Collection efficiency is the rate of accumulation of ice on any portion of the aircraft. It is also called the sticking efficiency which is the ratio of the particles that stick to the object to the particles that hit the object. The collection efficiency depends on the trajectory of each particle and the distance between particles and the distance on the surface where the particles may stick. When a super cooled drop hits an object it will freeze instantaneously. The sticking efficiency for snow particles depends on the conditions of the snow. Dry and hard snow will tend to bounce off whereas wet snow is very prone to stick upon impact, especially at low velocity and for certain temperature and humidity conditions.

- **Freezing fraction**

One of the most important non-dimensional parameters used in ice-accretion modeling is the freezing fraction. Freezing fraction sometimes referred to as accretion efficiency which is defined by the ratio of freezing ice mass to total water mass. If no

water freezes on impact, the freezing fraction will be measured as 0. If all particles freeze on impingement the accretion efficiency will be 1 and the ice is characterized as rime ice. If on the other hand the freezing rate is controlled by the transfer of the latent heat released during the freezing process the growth is characterized as being wet and the resulting ice is termed glaze ice.

- **Time of ice accretion**

The accreted mass of ice is clearly time dependent. Two identical ice storms of different duration will create different amounts of ice with the largest amount accreted in the longest lasting storm. The already accreted ice will change the flow field around the object and hence influence the collection efficiency. As the aircraft remains within icing cloud for a long duration, ice accretion will be more.

- **Aircraft surface temperature**

In order to form ice on any surface, the surface temperature must be at or below freezing temperature (0°C) at standard pressure (1 atm or 101325 Pa). If an aircraft has been in a region where temperature is below freezing and then it comes to a region above freezing temperatures, the aircraft's surface temperature can remain below freezing for some time. Therefore icing is possible in temperatures that are above freezing.

- **Airspeed**

As the airspeed increases, the number of water droplets struck by the aircraft surface increases in a certain period of time. At supersonic speed icing is not a severe problem and the concern of the aircraft designers is the excessive frictional and compression heating. But at subsonic speed the kinetic heating on the aircraft surface is of considerable interest to the aircraft designers.

1.3.3 Meteorological quantities

- **Liquid water content**

Liquid Water Content (LWC) is a measure of the amount of liquid water in a volume of air, often given in g/m^3. It depends on the classification of the cloud, elevation and temperature. Both rime and glaze can be produced for most of the values of LWC. This is due to the temperature dependency of LWC. Temperatures much below the freezing point will make the liquid water freeze and thereby reduce the LWC. The risk of an icing event increases with increasing LWC because there is simply more water which might freeze and accrete immediately.

- **Droplet size**

Droplet size is often given by the Median Volume Diameter (MVD), which is used as a single droplet size. The critical MVD for icing events is characterized by a droplet size of 1.5- 50 µm. Clouds and fog which have smaller droplet sizes than raindrops are able to super cool more and will therefore tend to accrete rime ice whereas larger super cooled drops are associated with glaze ice accretion.

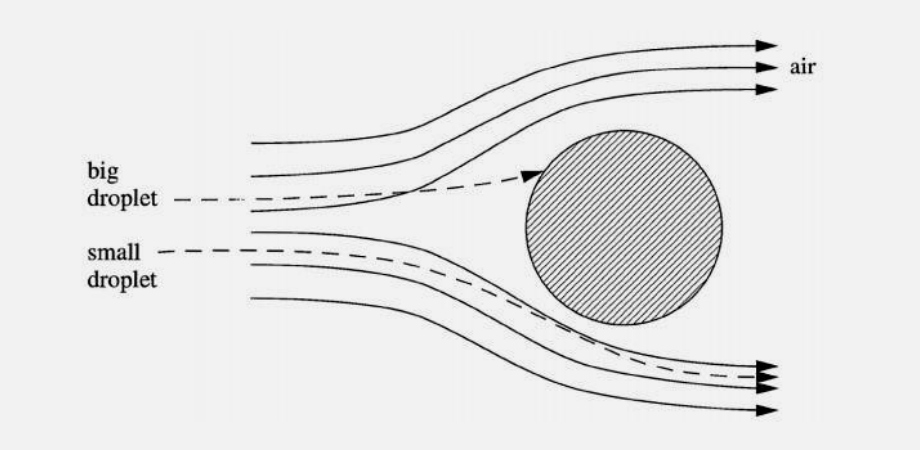

Fig. 1.5 Streamlines and droplet trajectories around a cylindrical object

- **Temperature**

Temperature is of course a very important factor in the field of icing. In general the risk of icing lies in an interval between zero and -15ºC. While the air temperature determines the state of the cloud, it is the liquid water content in the cloud that determines the icing threat as shown in the following chart.

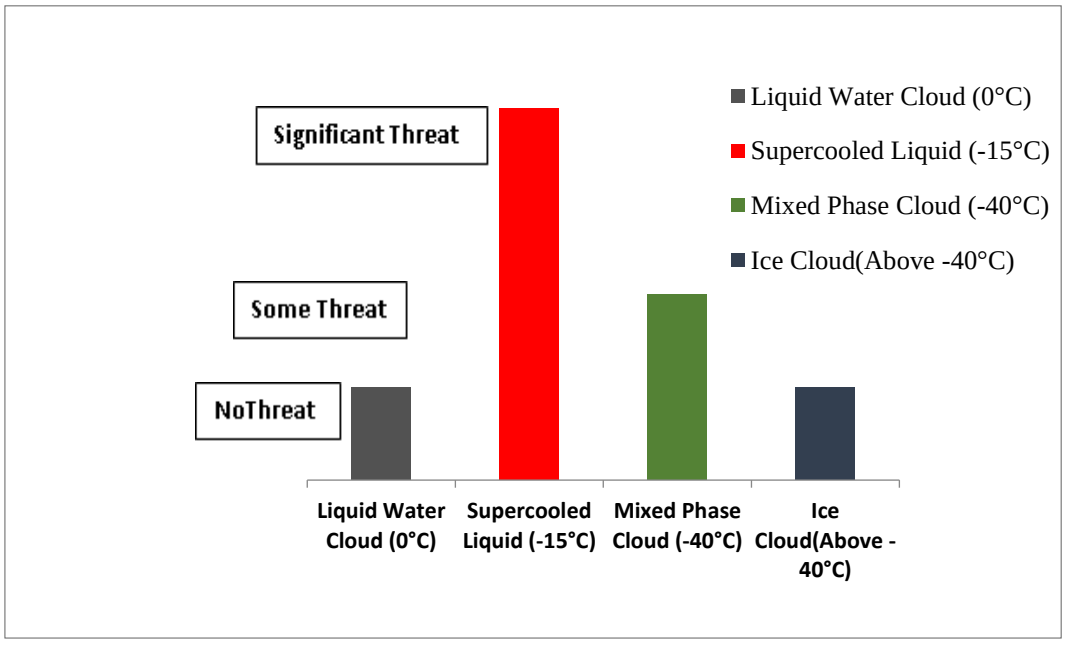

Fig. 1.6 Idealized cloud phase and icing threat

From the above chart, most significant icing threat occurs at altitude where air contains maximum super cooled liquid droplets and temperature ranges from -10 ºC to -20 ºC. From temperature range -20 ºC to -40 ºC some icing threat is present, as mixed phase clouds exist there. And for altitude where temperature is below -10 ºC and above -40 ºC, no icing threat is present.

1.3.4 Intensity of icing

The seriousness of an icing situation is, of course, dependent on the type of aircraft and the type of de-icing or anti-icing equipment with which the aircraft is equipped or the lack of such equipment. Clear ice is considered more serious than rime ice since the rate of catch must be high to precipitate the formation of clear ice. Basing on these factors icing may be described as light, moderate and severe (or heavy) [5].

Table. 1.1 Icing intensity classification

Intensity	Rate of accumulation
Trace	Perceptible, no significant accumulation
Light	Significant accumulations for prolonged flight (over 1 hour)
Moderate	Significant accumulations for shorter periods of flight
Severe	Rapid, dangerous accumulations

Table. 1.2 Icing intensity effects

Icing intensity	Airframe ice accumulation
Trace	Usually not hazardous event if de-icing/anti-icing equipment is not used.
Light	Occasional use of de-icing/anti-icing equipment removes/prevents accumulation.
Moderate	Rate of accumulation is such that event short encounters become potentially hazardous and use of de-icing/anti icing equipment or flight diversion is necessary.
Severe	De-icing/anti-icing equipment fails to reduce or control the hazard. Immediate flight diversion is necessary.

The icing intensity index used by the pilots and the icing intensity effects are mentioned in table. 1.1 and table. 1.2 respectively. Trace icing is perceptible and barely be seen. The rate of accumulation is slightly greater than the rate of sublimation. But icing is not

hazardous even if anti-icing or de-icing devices are not used. Light icing may create a problem if flight is prolonged for a long period of time. But occasional use of anti-icing or de-icing equipment may remove or prevent ice accumulation. For moderate icing the rate of ice accumulation even for a short period of time may be hazardous even after using anti-icing or de-icing devices. In case of severe icing intensity the anti-icing and de-icing devices fail to control the icing hazard and a flight diversion becomes necessary.

1.4 Types of Clouds and Precipitation

The types and intensity of in- flight icing is dependent on the tempreature and types of clouds and precipitation. According to the World Meteorological Organization (WMO) clouds can be classified into the following categories [41] which are described below:

1.4.1 High clouds (20,000 ft or above British Isles)

- **Cirrus clouds:** Cirrus clouds are short, detached and hair like clouds found at high altitudes. In day time they are whiter than any other clouds. While the sun is setting or rising, they may take on the colors of the sunset.
- **Cirrocumulus clouds:** Cirrocumuls clouds are extended over 20,000 ft to 40,000 ft above base. They are made of a number of small white clouds called cloudlets and are grouped together at high altitudes. They are composed from almost entirely ice crystals, the little ice crystals are regularly spaced, often arranged as ripples in the sky.
- **Cirrostratus clouds:** These clouds are transparent high clouds and cover a large portion of the sky. They sometimes produce white or colored rings around the sun or moon known as halo phenomena. Sometimes they are so thin that the halo is the only indication that a cirrostratus cloud is in the sky.

1.4.2 Medium cloud (between 6,500 ft and 20,000 ft over British Isles)

- **Altocumulus clouds:** Altocumulus clouds have height of base from 7,000 ft to 18,000 ft and are small mid- level layers of clouds. They most commonly exist in the shape of rounded clumps. Altocumulus clouds can appear in a variety of shapes and are mixed up of ice and water.
- **Altostratus clouds:** Altostratus clouds are extended over 6,500 ft to 20,000 ft from base. They are large mid- level sheets of thin clouds usually

composed of a mixture of water droplets and ice crystals. They are thin enough that the sun can be seen weakly through the cloud. Altostratus clouds are often spread over a large area and are usually featureless.

- **Nimbostratus clouds:** They are extended over 10,000 ft from the base and are usually dark, grey, featureless layers of clouds and are thick enough to block out the sun. These clouds often produce persistent rain and probably are the least picturesque of all the main cloud types.

1.4.3 Low clouds (below 6,500 ft over British Isles)

- **Stratocumulus clouds:** Stratocumulus clouds have coverage up to 6,500 ft from the base and are low- level patches of cloud varying in color from bright white to dark grey. They are the most common clouds that can be recognized by their well-defined bases. Stratocumulus clouds are formed when stratus clouds are embedded with cumulus clouds.
- **Stratus clouds:** Stratus clouds are low- level layers of clouds with a fairly uniform grey or white color. They can persist over a long period of time of the day. They are the lowest lying cloud type and sometimes appear at the surface in the form of mist or fog.
- **Cumulus Clouds:** Cumulus clouds are extended over a range of 1200 to 6,500 from base and are generally detached, individual, cauliflower-shaped clouds usually spotted in fair weather conditions. The top of the clouds are usually relatively dark.
- **Cumulonimbus clouds:** Cumulonimbus clouds are generally multi- level clouds, extending high into the sky. More commonly known as thunderclouds, cumulonimbus are the only cloud type that can produce thunder and lighting. The base of the cloud is often flat with a very dark wall like feature and they lie only a few hundred feet above the earth surface.

1.5 Icing Effects on Aircraft Performance and Control

Ice on aircraft aerodynamic surfaces can lead to loss in lift, increase in drag, and early stall. It can also severely alter the stability and control characteristics of the aircraft [7]. Ice collects on and seriously hampers the function of not only wings and control surfaces and propellers, but also windscreens and canopies, radio antennas, pitot tubes and static

vents and air intakes. Ice on the engine rotor and stator blades affects their performance and efficiency and may result in flame out. Vibration of ice breaking off may be sucked into the engine and cause structural damage. Icing occurred at the time of take-off and landing may obscure the runway and other landmarks causing severe accidents.

If ice builds up on the pitot tube and static pressure ports, flight instruments may cease operating. The altimeter, airspeed and rate of climb would be affected displaying confusing readings. Gyroscopic instruments powered by a venturi would be affected by ice building up on the venturi throat. Ice on radio antennas can impede VOR reception and destroy all communications with the ground. Whip antennas may break off under the weight of the accumulating ice.

Icing is extremely dangerous if it is happening on the unprotected aircraft surfaces like wings, tail surfaces and other projections resulting in disruption of the airflow around the wings and tail surfaces. The ice changes the airfoil cross section and destroys lift, increases drag and raises the stalling speed. At the same time, thrust is degraded because of ice on the propeller blades. In a nutshell if ice accretion is prolonged, excessive decrease in lift and increase in drag cause the aircraft to lose altitude. Excessive drag increase will cause the aircraft to lose airspeed and lift and stalling at an early angle of attack. And the pilot has to use full engine power and a high angle of attack just to maintain altitude. Thus retardation in aerodynamic performance of the aircraft results in from ice accumulation.

1.6 Existing Ice Protection System

The need for all weather operation of the aircraft requires the correct detection of several environmental threats like freezing rain, ice accretion, presence of super cooled droplets etc. In order to cope with the icing hazards necessary measures are required to sense and detect the ice formation at different parts of the aircraft. The very first attempt in this regard is the prediction of weather condition. So most of the aircrafts now are equipped with Airborne Weather Radar (AWR) system that can provide a weather picture ahead of the aircraft and helps to identify and avoid specific, adverse weather conditions that can lead to ice accretion.

To protect the aircraft from icing the following methods are used [7]:

- If icing occurs before take- off it is removed using de- icing fluid, mechanical means or using infrared heating.

To protect an aircraft against icing in-flight, the following anti-icing or de-icing techniques are used:

- Most common approach is to route the engine bleed air to the icing surface to melt or evaporate the ice.
- Some of the aircrafts have pneumatic de- icing boots that disperse ice build- up on the surface.
- Very few aircrafts are equipped with weeping wing system with hundreds of holes on the wing and tail leading edges that release anti- icing fluid to prevent icing in case of emergency.
- Most modern anti- icing system used now- a days is the electro- thermal anti-icing system that provides continuous heating but is used for the most sensitive and small aircraft components.

1.7 Objectives

In all cases use of anti- icing or de- icing devices are usually utilized for only the critical aircraft surfaces and components. In particular the aircraft surface and structural components remains usually unprotected. Hence design of an efficient anti- icing and de-icing device for the structural components like wings, tail surfaces requires the estimation of the ice accretion under various environmental conditions.

Thus the objective of the research is:

- To study the performance of a NACA 2412 (base airfoil) in dry condition by Computational Fluid Dynamics analysis.
- To calculate the leading edge ice accretion thickness of a NACA 2412 airfoil based on the quantitative analysis of a two- dimensional ice accretion method and Messinger freezing fraction model.
- To obtain distorted airfoil shape due to ice accretion by varying the different parameters such as freezing fraction (0.3 to 1.00), time of ice accretion (200s to 1000s) and Reynolds number (5×10^6 , 6×10^6 , 8×10^6 and 15×10^6).
- To compare and analyze the aerodynamic performance of ice accreted airfoil against base airfoil using CFD technique.

The possible outcome of the research is:

- To provide an input for the design of an efficient anti- icing and de- icing device for high altitude flights.

1.8 Motivation behind the Present Study

Present research work gives an overview of aircraft icing risk and its impacts on flight safety and economy. This discussion includes the factors influencing in-flight icing and the effects of ice formation on aircraft performance. Although major advancements in aircraft ice protection systems have been made over the years, accidents due to icing are still occurring. To cope with ice accretion, many airplanes are equipped with anti/de-icing devices. However, due to installation, maintenance costs and weight issues, the operation of these devices is limited to small portions of the surface for as little time as possible. Therefore, the device should be designed for high efficiency. Implementing an efficient anti/de-icing device requires estimation of the accurate ice accretion profile, the heat capacity of the surface to eliminate the ice. These characteristics related to icing are available through researches into the icing behavior. The investigation into icing behavior and its aerodynamic effects can be conducted by an experimental method or by numerical analysis. Experimental studies may take the form of flight tests or icing wind tunnel tests. In a flight test, the air-plane has to actually fly through the area in which the icing occurs. Therefore, the difficulties involved in running flight tests are forecasting the conditions under which icing occurs; capturing, recording, and controlling the icing behavior, safety and cost. The icing wind tunnel test is limited by the cost of acquisition and maintenance of the facility, in addition to scaling problems if a subscale model is used. Therefore, in order to understand the ice accretion behavior under various icing conditions and estimate the reduction in aerodynamic performance of the wing, this research has relied on simulation codes rather than experiments.

1.9 Applications

This research contributes by developing a numerical model designed to generate more efficient in- flight anti- icing and de- icing devices based on estimation of the real life in-flight ice accretion estimation. To this end, a numerical tool was developed to explore the aircraft behavior in real weather icing scenarios. The tool allowed an independent assessment of the methodology based on the primary estimation of ice and aerodynamic performance degradation under various icing conditions. Data sets of this nature will help the pilots in pilot training or engineering evaluation of system failure impacts or control system design. Overall, the research contributes by combining concepts of in-flight icing fundamentals and aerodynamic performance of the icing surface as a safety issue.

CHAPTER 2

LITERATURE REVIEW

2.1 Overview

Chapter 2 gives an overview of the literature studies carried on relevant subject concerning aircraft in- flight icing, the effects of various parameters leading to ice accretion and aircraft aerodynamic performance under icing conditions. This chapter mainly presents the experimental, analytical and computational research work undertaken post 2nd world war to the recent time. This chapter also highlights the studies on available de-icing / anti- icing devices, their efficiencies in ice removal during flights and icing codes and models available to predict airfoil leading edge ice accretion. This chapter concludes with a study case in this research field based on the identified areas that require further improvements.

2.2 Experimental Studies

Research activities on aircraft icing had started from the late 1920s and early 1930s but extensive experimental research using wing tunnel had started just after the Second World War. The earliest recorded experimental studies on in- flight icing was carried out by Gulick [8] in 1938 tested a 6 aspect ratio wing in the Langley Full-Scale Tunnel with leading edge ice roughness. He had measured a 25% reduction in maximum lift and a 90% increase in drag for the tested icing conditions. Bowden [9] in 1956 presented a fairly complete aerodynamic evaluation of icing effects on a NACA 0011 airfoil. A six-component force balance system was used to enable the measurement of changes in lift, drag, and pitching moment. Gray [10] conducted a series of experiments where ice was accreted under carefully controlled conditions. The ice accreted shapes were recorded as well as changes in lift, drag, and pitching moment. Icing conditions were varied to study the effect of droplet size, liquid water content, air temperature, icing time, and angle of attack.

In the early 90s there was significant interest in ice and frost roughness effects on airfoil and wing aerodynamics while much of the aerodynamic research in this period focused on large ice accretions. Local heat transfer coefficients were measured by Poinsatte [11] for both smooth and roughened NACA 0012 airfoil in- flight on the NASA Lewis Twin Otter Research Aircraft and in NASA Lewis Icing Research Tunnel based on the ice accretion thermal physics. By the mid-90s numerous experimental studies had been

carried out to examine the case of an airfoil with a large glaze ice shape and the fundamentals of the flow field with its large separation region were recorded. The ATR-72 accident in the late 1994 changed the focus of aerodynamic icing research. Icing research focus was renewed in performance testing of airfoils and wing geometries with ice contamination. In 1997, Kerho and Bragg [12] performed detailed studies on the boundary-layer development on ice accretion on the leading-edge of an airfoil. This research showed that roughness due to ice accretion did not immediately cause boundary-layer transition but initiated the transition process that developed slowly downstream. This had implications for heat transfer modeling in ice accretion codes.

A major change in this research field was the consideration of various airfoil sections for a better understanding of the effect of icing on airfoil geometry. In 1999, a systematic study was carried out by Bragg et al [13] on the effects of simulated ice shape geometry on airfoil aerodynamic performance. Experimental investigation was conducted in wind tunnel with a NLF (l)-0414 airfoil. Several configurations with glaze ice geometry were studied varying the Reynolds number, leading edge radius and size of airfoil. Reynolds number was found to have little effect on the aerodynamic results on the airfoil with simulated ice shapes. Anderson [14] in 2003 evaluated and validated the freezing fraction (a non-dimensional parameter)for calculating leading edge ice accretion. The icing tests were performed in NASA Glenn IRT for a NACA 0012 airfoil under several test conditions which show a good agreement of the analytical freezing fraction value with the experimental one. A low- speed, low- turbulence wind tunnel test was carried out by Broeren et al [15] to evaluate the performance effects of inter cycle icing on three different airfoil sections. The study showed that a simple geometric (chord-based) scaling of the ice was appropriate. However some other important parameters like collection efficiency affecting the ice accretion process were not addressed in this study which was addressed by Bidwell et al [16] in their work in 2005.

In addition to the primary aerodynamic performance degradation, icing may affect the aircraft control and stability. Effect of icing on aircraft stability and control were addressed by Lee et al [17] by conducting numerous wind tunnel tests on a number of two-dimensional airfoil models and some three-dimensional wing and tail models. Icing scaling tests were carried out in NASA Glenn Icing Research Tunnel (IRT) by Tsao [19] to assess the scaling method for aircraft wings application. However, this method of traditional ice tracing was not sufficient to characterize the three dimensional ice features.

An extensive experimental work was conducted by Han [18] in 2013 on rotor-ice-accretion and corresponding wind-tunnel aerodynamic testing to provide an independent data set for the validation of the analytical method known as Han–Palacios Correlation (HPC). A full-scale wind tunnel test was carried out by Andreev G.T et al [1] on a semi span wing of Yak-40 to investigate the icing effects on aerodynamics characteristic of aircraft. Several experiments were conducted by Pouryoussefi et al [20] in a low-speed, open-circuit wind tunnel in the aerospace engineering department at K.N. Toosi University of Technology. The study was carried out on the effects of different forms of ice horn, runback, and span wise ridge ice at varying angles of attack on a NACA 23012 airfoil section. The study concluded that span wise ice formation is the most hazardous for the aircraft hampering the reliable operation of anti-icing and de-icing devices. The ice accretion and aerodynamic testing in the Modern Airfoils Program was described in more detail for the NREL S826 airfoil in icing conditions [21].

Significant investment in iced-aircraft aerodynamics was made by studying the ice accretions on unprotected airfoil surfaces and the performances of the de- icing and anti-icing devices. Till now significant icing aerodynamics experimental researches were conducted and continue up to this writing.

2.3 Analytical Studies

This review includes the added details of past to the recent works that are more focused on ice accretion flow field physics. Early analytical research focused primarily on calculations of the flow field and performance of airfoils with large glaze-ice horns. Some of the earliest calculations were performed by Langmuir and Blodgett [22] to determine the trajectories of small water droplets in air moving at high velocities across a cylinder. An analytical model was used to calculate the trajectories for the case of air flowing around a sphere. A complete analysis of the temperature of an unheated surface in icing conditions was presented by Messinger [23] for several significant regimes (i.e., less than 32°F. , at 32°F. , and above 32°F.) as a function of air speed, altitude, ambient temperature and liquid water content. Curves were presented to determine the speeds beyond which no ice accretion will occur. Curves were also presented to indicate the surface temperature and the rate of ice sublimation which takes place when an ice-covered surface emerges into clear air. One significant result of this study is the

introduction of a new basic variable referred to as the "freezing-fraction," which denotes the proportion of the impinging liquid which freezes in the impingement region.

Shin et al [24] introduced the Interactive Boundary-Layer (IBL) method to predict ice shapes and their effects on airfoil performance. The IBL method couples the solutions of inviscid and viscous flow equations so as to ensure that each influences the other. However, this model lags the additional measurements and calculations that are required to examine the sensitivity of the aerodynamic flow characteristics to the time change in ice shapes.

With the passage of time, a number of parameters like wing geometry, airspeed, freezing fraction, collection efficiency, liquid water contents etc. had been identified as important factors in determining ice shape. But there had been only a few studies that have attempted to evaluate how each parameter affects the ice shape or how closely scale and reference values of the parameters must agree. Anderson et al [25] had made a systematic study of these similarity parameters used in icing scaling by examining the physics of icing. And they concluded that similarity of each of several processes like flow field, droplet motion, non-dimensional water-film thickness and total ice accretion need to be maintained between the scale and the reference situations. Fortin et el [26] presented the new improvements on numerical ice accretion model by comparing mass and shape of ice accretion which was a combination of thermodynamic model, roughness model and mass model. This analytical model had shown better agreement with the experimental data compared to the existing icing models.

Various physical models for ice accretion had been developed since 1950's with the purpose of designing anti-icing systems. Basically these icing models consist of solving the external flow equation and computing the water impinging flux on the surface hence the collection efficiency calculation. Silveira et al [27] in their research had compared the Lagrangian model, Eulerian model and Passive scalar transport model for calculating the collection efficiency. The analysis concluded that Lagrangian model is more appropriate to calculate the collection efficiency for simple 2D geometry while the Eulerian approach is more applicable for complex geometries. Yee et al [28] presented the development of an analysis code for icing behavior under rime ice and glaze ice conditions. The code consisted of Messinger's model and an aerodynamic solver that employed the panel method and boundary layer theory. The accuracy of the code was verified objectively

through quantitative investigation and the behavior of ice accretion was characterized. In addition, the influence of ambient conditions on icing behavior was investigated in terms of the selected parameters and came to the conclusion that the free stream velocity was the factor that had the greatest influence on the behavior of ice accretion at a given temperature.

The above discussed icing models have considered the icing properties as constant. However, there exists two modes for aircraft icing, i.e. the dry and the wet mode icing was addressed by Zhang et al [29] in the year 2016. Rime ice forms on aircraft skin during the dry mode icing while Glaze ice forms on the rime ice when water film appears on the glaze ice during the wet mode icing. The new one- dimensional model developed by them based on the fundamental theory of solid-liquid phase change was popularly known as the Property-Variable Rime Ice (PVRI) model. This universal model thus concluded that the ice accretion process is affected by the airflow parameters as well as the heat conductions in the ice layer and water film, which are influenced by the rime ice physical properties. One of the fundamental drawbacks of this model is the exclusion of runback water effect which was considered in their next model termed as PVRI- RW model [30].

These analytical methodologies with additional empirical corrections may subsequently be used to reduce the cost of experimental set up, number of flight tests as well as help development of numerous computational tools.

2.4 Computational Studies

As the computational power increased and turbulence modeling and grid generation improved, the Interactive Boundary-Layer (IBL) technique gave rise to ever more sophisticated methods. By 1990 Computational Fluid Dynamics (CFD) method based on the Navier- Stokes equation to describe the aerodynamics of iced airfoils and wings came into existence. The CFD modeling has emerged as a powerful tool for the prediction of ice shapes and for the simulation and optimization of the ice protection systems. Currently various icing codes have been developed most of which provide simplified roughness modeling through the use of empirical correlations.

A computer code named LEWICE was developed at NASA Lewis which could accurately predict ice growth under any meteorological conditions for any aircraft. This computer code is actually an analytical ice accretion model that evaluates the

thermodynamics of freezing process when ice is accreted on any surface. This code consists of four major modules: calculation of flow field, calculation of trajectory, calculation of ice growth and modification of the geometry by addition of the ice growth. Wright in 1999 presented validation of the LEWICE 2.0 code with experimental data from NASA IRT [31]. And the difference between the predicted ice shape from LEWlCE 2.0 and average of the experimental data was only 7.2% for geometric characteristics of over 100 ice shapes.

Yung and Mary [32] had rightly identified two major problems related to aircraft icing. One is predicting the effects of ice on the aerodynamic performance of airfoils when ice geometry is known and the other one is simulating ice accretion under specified icing conditions and had addressed two identical software in their research work. SmaggIce was being developed for the simulation of "icing effects" on airfoil aerodynamic performance and ICEG2D was developed for ice accretion simulations. All these software can predict ice accretion for many cycles of geometry modeling/grid generation/flow simulations.

A second generation in- flight icing simulation code was developed by Habashi et al [33] for calculating ice shapes on simple or complex 3D geometries. The resulting ice simulation system, FENSAP-ICE, was designed in such a way that it can successively solve each of flow, impingement and accretion via field models based on partial differential equations (PDEs). The code was validated for other codes available in open literature. Croce et al [34] made the use of quantitative and phenomenological data that enables the numerical prediction of time accretion for ice formation by developing an unsteady ice accretion simulation technique embedded in FENSAP-ICE. This study extended the applicability of FENSAP-ICE outside the range of airfoil types. However, a further development of the technique requires the investigation of the interaction between growing roughness and impinging droplet.

Computational ice accretion methods including LEWICE and ONICE had been used to guide the experiments and were briefly described by Bragg et al [35]. When full-scale and simulation aerodynamic results are available, these data can be used to further development of computational tools. Tabatabaei et al [36] used a Computational Fluid Dynamics (CFD) model to study the effects of "critical ice accretions" on the aerodynamic properties of the iced profile and validated the results with experimental

data.. Grid topology of C-type was used to generate high quality structured hexahedral grid by ICEM CFD15. Numerical simulations were performed using ANSYS CFX 15.0. Both steady state and transient simulations were conducted. High-resolution advection scheme was selected for the spatial discretization and 'Second Order Backward Euler' scheme was applied for the temporal discretization of RANS equations. Shear stress transport model with automatic wall function was activated to model the turbulent flow. The computational results very well converged with the experimental results available in open source.

A recent study was carried out in 2017 by Hanson and Kinzel [37] on LEWICE- based ice shape prediction coupled to a computational fluid dynamics (CFD) model using a Discrete-Element Roughness Method (DERM) prediction of heat transfer. Comparisons of ice-shape predictions and aerodynamics were made between the experimental, SGR-LEWICE, and DERM-LEWICE to evaluate the benefit of an improved heat transfer prediction methodology. The results indicate that the DERM model provides an improved prediction of heat transfer relevant to ice roughness.

2.5 Summary of Literature Review

The above literature review in a nutshell summarizes that significant experimental, analytical and computational research on icing aerodynamics had been conducted till today. However, in the literature most of the studies focused on a particular airfoil section considering icing property as constant. Though with the passage of time various parameters were identified which directly affect the icing behavior very few studies had attempted how closely each of these parameters affects the ice shape. Moreover, much information is not available about the real time ice accretion behavior under various cloud conditions and altitude variation. Though various physical models had been developed with a view to designing anti- icing and de- icing devices, very little information is available about the effects of varying ambient conditions on a fixed geometry or the effects of varying geometry for specific conditions. Considering this fact, the scope of this thesis is to develop a numerical code to investigate the effects of various parameters on ice accretion identified previously in different literature. The study also aims at considering different altitude levels hence varying temperature and cloud conditions and other ambient conditions for designing of efficient in- flight anti-icing and de-icing devices.

CHAPTER 3

NUMERICAL MODEL AND VALIDATION

3.1 Overview

This chapter discusses the methodologies to describe the approach to the research problem and the principles of methods and tools used in achieving the objectives of this research. This chapter also highlights the validation of the proposed model using the experimental data from the open source.

3.2 Existing Analytical and Numerical Models

Literature review on the current research had shown that the recent advancements in technology have provided the development of several analytical and numerical tools for predicting the in- flight leading edge ice accretion for different parts of the aircraft. Some of the conventional analytical models include the Interactive Boundary Layer (IBL) Method, Thermodynamic Model, Roughness Model and Mass Model, Lagrangian Model, Eulerian Model, Passive Scalar Transport Model and most recent PVRI and PVRI- RW model.

The available computational tools are LEWICE, SmaggIce, ICEG2D, ONERA, CIRA, IMPIN3D, DRA and FENSAP-ICE. All these analytical and numerical models can predict the ice accretion physics studying the water droplet trajectories and collection efficiency and other parameters. However, as the geometry of the icing surface changes the ice accretion physics as well as the aerodynamic performance of the surface also changes. The approach in this work, therefore, is to develop a numerical code and CFD model that includes the icing conditions to demonstrate the environmental effects and also the performance degradation for a NACA 2412 airfoil due to the ice accretion of different levels.

3.3 Proposed Model

3.3.1 Numerical Model

Although there are many different numerical analysis tools, every icing behavior analysis and icing prediction code requires the following models:

i. A model that can calculate the velocity vector around the wing or airfoil.

ii. A model that calculates the trajectory of water droplets.

iii. A model that can determine the amount of liquid water that inflows on to the surface.

iv. A thermodynamic model that determines the mass and energy conservation within a control volume.

v. A model that determines the ice thickness.

vi. A model that generates the distorted airfoil shape.

As mentioned earlier, the icing behavior is influenced by various parameters, this study selects the free- stream velocity, ice accretion time, and freezing fraction as the principal parameters. In this study a numerical analysis code that can predict the leading edge ice accretion was developed based on the following models:

A numerical model was developed that can determine the thickness of the ice mass accreted on airfoil surface and the distorted airfoil shape at the ambient conditions. To proceed with this model initially a control volume was established on the airfoil surface as shown in fig. 3.1.

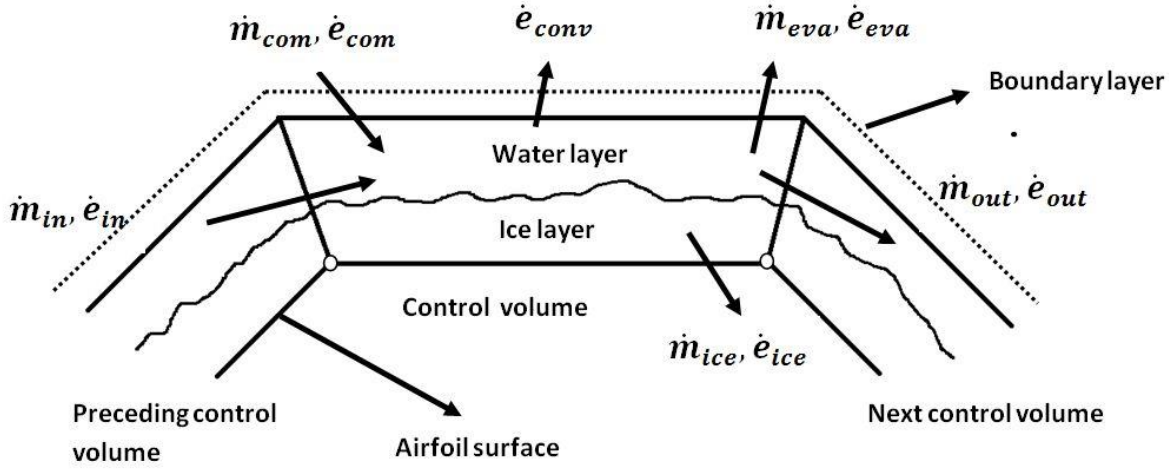

Fig. 3.1 Mass and energy conservation within a control volume

The mass and energy are conserved within the control volume as per the following mass and energy conservation equations [28]:

$$\dot{m}_{com} + \dot{m}_{in} = \dot{m}_{ice} + \dot{m}_{out} + \dot{m}_{eva} \quad (3.1)$$

$$\dot{e}_{com} + \dot{e}_{in} = \dot{e}_{ice} + \dot{e}_{out} + \dot{e}_{eva} + \dot{e}_{conv} \quad (3.2)$$

Each of the terms in the above equations can be determined using the equations (3.3) to (3.11):

$\dot{m}_{com}$ is the mass of impinging water that inflows onto the surface. As it is not possible to directly determine the mass of impinging water, it is calculated indirectly using the collection efficiency [28]. As shown in fig. 3.2 collection efficiency is the ratio of the distance Δy between particles and the distance ΔS on the surface where the impinging particles may stick.

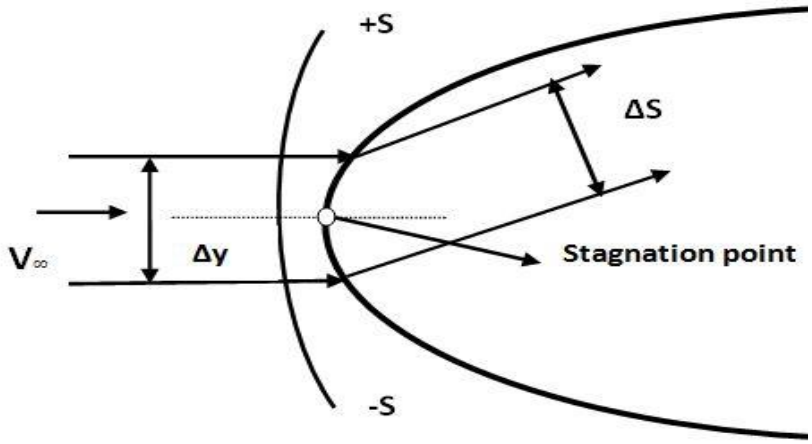

Fig. 3.2 Water droplet trajectory (Close up view)

Thus assuming that the particles are uniformly distributed in the air, the mass inflow of the liquid water from air to the surface is determined by the following equation (3.3):

$$\dot{m}_{com} = \Delta y . LWC . V_{\infty} \tag{3.3}$$

Where,

$\beta = \frac{\Delta y}{\Delta S}$ is the collection efficiency or catch rate or rate of ice accumulation on the surface.

LWC is the liquid water content in the air that depends on the temperature condition and cloud type.

V_{∞} is the free stream air velocity.

ΔS is the distance on the surface where the droplet particles strike.

Next term in the left hand side of equation (3.1) is the $\dot{m}_{in}$, that is the mass of runback water into the control volume from the previous control volume. As we started our

calculation, the initial $\dot{m}_{in}$ was considered to be zero beacuse there was no previous control volume that transfers water mass.

The quantities at the right hand side of the equation (3.1) are the evaporated water mass, ice mass and runback water mass to the next control volume. Evaporation water mass is the function of surface temperature and can be determined using the following equation [38]:

$$\dot{m}_{eva} = \frac{.7}{C_{Pa}} h_c \left(\frac{P_{v,sur} - P_{v,sur}}{P_\infty} \right) \tag{3.4}$$

Where,

$C_{Pa}$is the specific heat of air.

$h_c$is the convective heat transfer coefficient which can be determined from the Nusselt number as follows [14]:

$$h_c = \frac{k_a N_u}{d} \tag{3.5}$$

Here, d is the leading edge diameter of the airfoil. Poinsatte [11] had measured the heat transfer coefficients at the stagnation line of an NACA 0012 airfoil at the IRT using the chord length as the characteristic length. But to cope up with the practice in this study leading edge diameter of the airfoil is considered as the characteristic length and Poinsatte expression becomes:

$At\ 0 \deg AoA,$ $$N_u = 1.10 {R_e}^{.472} \tag{3.6}$$

$P_{v,sur}$and $P_{v,\infty}$are the vapour pressure at the ice or water surface and for ambient air respectively. These are computed from the following equations:

$$P_{v,} = 3386(.0039 + 6.8096 \times 10^{-6} \bar{T}^2 + 3.5579 \times 10^{-7} \bar{T}^3 \tag{3.7}$$

$$\bar{T} = 72 + 1.8(T - 273.15) \tag{3.8}$$

The other two quantities ice mass and runback water mass can be determined as per equation (3.5) and (3.6) using the freezing fraction which is the ratio of the freezing ice mass to the total ice mass and was first studied by Messinger [23].

$$f = \frac{\dot{m}_{ice}}{\dot{m}_{com} + \dot{m}_{in}} \tag{3.9}$$

$$\dot{m}_{ice} = f(\dot{m}_{com} + \dot{m}_{in}) \tag{3.10}$$

$$\dot{m}_{out} = (1-f)(\dot{m}_{com} + \dot{m}_{in}) - \dot{m}_{eva} \quad (3.11)$$

From the energy conservation equation of equation 3.2, the energies coming from the air, adjacent control volume and moving to the next control volume are calculated using the following equations:

$$\dot{e}_{com} = \dot{m}_{com}[\ c_{p,w}(T_{sur} - T_i)\frac{{V_\infty}^2}{2}] \quad (3.12)$$

$$\dot{e}_{in} = \dot{m}_{in}[\ c_{p,w}(T_{sur(I-1)} - T_i)] \quad (3.13)$$

$$\dot{e}_{eva} = \dot{m}_{eva}[\ c_{p,w}(T_{sur} - T_i) + L_v] \quad (3.14)$$

$$\dot{e}_{conv} = h_c[\ T_{sur} - (T_e + \frac{r_h {V_\infty}^2}{2c_{p,a}})]\,\Delta S \quad (3.15)$$

$$\dot{e}_{ice} = \dot{m}_{ice}[\ c_{p,i}(T_{sur} - T_e) - L_f] \quad (3.16)$$

$$\dot{e}_{out} = \dot{m}_{out}[\ c_{p,w}(T_{sur} - T_i)] \quad (3.17)$$

Where,

$c_{p,w}$ and $c_{p,i}$ are the specific heat of water and ice respectively.

L_f and L_v are the latent heat of fusion and latent heat of evaporation respectively.

At the beginning of the calculation all the terms of equation (3.1) are substituted in equation (3.2).Values of all the constant terms are used for the ambient condition [39]. So, the resulting equation is left with only two unknown terms, surface temperature $T_{sur}$and the freezing fraction, *f*. These two quantities are now calculated using an iterative process.

For the initial iteration, the surface temperature is considered to be the freezing point i.e 273.15 K and *f* is calculated. If it is found that $f < 0$, it implies that the surface temperature is greater than 273.15 K, so f is set to be 0 and T_{sur} is calculated again. On the other hand, if it is found that $f > 1$, it implies that the T_{sur} is greater than 273.15 K, so f is set to 1 and T_{sur} is recalculated. If two successive iterations give the T_{sur} value close to each other, then only T_{sur} and f are known and $\dot{m}_{ice}$, $\dot{m}_{out}$ and $\dot{m}_{eva}$ are found for each of the control volume.

Next step is the calculation of the height of ice growth for each surface panel of length ΔS. During a small time interval Δt, the height of ice growth on each surface panel is

determined based on the ice mass calculated in the previous step using the following equation (3.18) [28]:

$$h = \frac{\dot{m}_{ice}.\Delta t}{\rho_{ice}.\Delta S} \tag{3.18}$$

Where, ρ_{ice} is the density of ice.

Finally, based on the assumption that ice grows only in the normal direction to the airfoil surface, these ice growth heights are then added normal to the surface panels to produce a new surface profile. As the time interval increases, the ice growth becomes more and thus generating distorted airfoil shapes due to ice accretion.

3.3.2 Numerical code

Combining the above models a numerical analysis code was developed and the code was solved using MATLAB 14.0 software. This code can determine the ice thickness accreted on an airfoil emphasizing the ice accretion time and freezing fraction at various icing conditions and also can generate the distorted airfoil shape. Moreover, the code was also modeled for observing the effects of variation of Reynolds number at the same icing conditions.

3.3.3 CFD (Computational Fluid Dynamics) model

For the development of an efficient anti-icing or de-icing device for the aircraft and certificate of airworthiness, it is essential to predict the ice accretion shapes and the aerodynamic performance in various icing conditions. For understanding the flow field and degradation in the aerodynamic performance around the ice accreted airfoil a Navier-Stokes equation based CFD model was used. Considering the time factor a 2D geometry of the airfoil was considered. In order to observe the flow field around the iced airfoil a standard k-ε turbulent model was used. As the ice profile produced more complex geometry of the airfoil, much attention was given to produce a better quality grid system. For the CFD analysis ANSYS Fluent 16.0 was used as the computational tool.

3.3.3.1 Governing Equations

The Navier-Stokes equation which describes the motion of viscous fluid substances is the governing equation of Computational Fluid Dynamics (CFD). It is based on the conservation law of physical properties of fluid. Applying the mass, momentum and

energy conservation, the continuity equation, momentum equation and energy equation can be derived as follows[40]:

Continuity Equation:

$$\frac{D\rho}{Dt} + \rho \frac{\partial U_i}{\partial x_i} = 0 \tag{3.19}$$

Momentum Equation:

$$\rho \frac{\partial U_j}{\partial t} + \rho U_i \frac{\partial U_J}{\partial x_i} = -\frac{\partial P}{\partial x_j} - \frac{\partial \tau_{ij}}{\partial x_i} + \rho g_j \tag{3.20}$$

Where,

1st term: Local change with time

2nd term: Momentum convection

3rd term: Surface force

4th term: Molecular-dependent momentum exchange (diffusion)

5th term: Mass force

And

$$\tau_{ij} = -\mu\left(\frac{\partial U_j}{\partial x_i} + \frac{\partial U_i}{\partial j}\right) + 2/3\,\delta_{ij}\mu\frac{\partial U_k}{\partial x_k} \tag{3.21}$$

Energy Equation:

$$\rho c_\mu \frac{\partial T}{\partial t} + \rho c_\mu U_i \frac{\partial T}{\partial x_i} = -P\frac{\partial U_i}{\partial x_i} + \lambda \frac{\partial^2 T}{\partial x^2} - \tau_{ij}\frac{\partial U_j}{\partial x_i} \tag{3.22}$$

1st term: Local energy change with time

2nd term: Convective term

3rd term: Pressure work

4th term: Heat flux (diffusion)

5th term: Irreversible transfer of mechanical energy into heat

To simplify the Navier-Stokes equations can be rewritten as the general form:

$$\frac{\partial(\rho\varphi)}{\partial t} + \frac{\partial}{\partial x_i}\left(\rho U_i\,\varphi - \Gamma_\varphi \frac{\partial \varphi}{\partial x_i}\right) = q_\varphi \tag{3.23}$$

3.4 Validation of the Ice accretion and CFD Computations

In order to verify the results of ice accretion calculations and aerodynamic data generated by the CFD are correct and credible, there is requirement to validate the CFD results with experimental results. Since the objective of present thesis is only computational analysis, therefore, the ice accretion over airfoil and CFD validation is undertaken with open source data. Therefore following experimental data available from open source is utilized to validate the ice accretion

3.4.1 Description of the Experimental Set Up for ice accretion validation

Han and Palacios [18] undertook experimental study of ice accretion over the rotor blades in the Adverse Environment Rotor Test Stand (AERTS) facility of the Pennsylvania State University followed by the wind tunnel analysis of the ice accreted airfoil. For the experimental study Han and Palacios [18] considered two blade configuration of helicopter rotor having the blade cross section of NACA 0012. The ice accretion was undertaken for different environmental and icing conditions (such as temperature, density, LWC and icing time etc). The blades had a diameter of 2.7 m while chord length of 0.533 m. The rotor rpm could be varied between 200 to 1200 rpm. The test stand was built inside a cold chamber that was capable of maintaining constant temperatures ranging from 0 to −25 °C during icing tests. Experimental set-up of the icing study is shown in fig. 3.3 below.

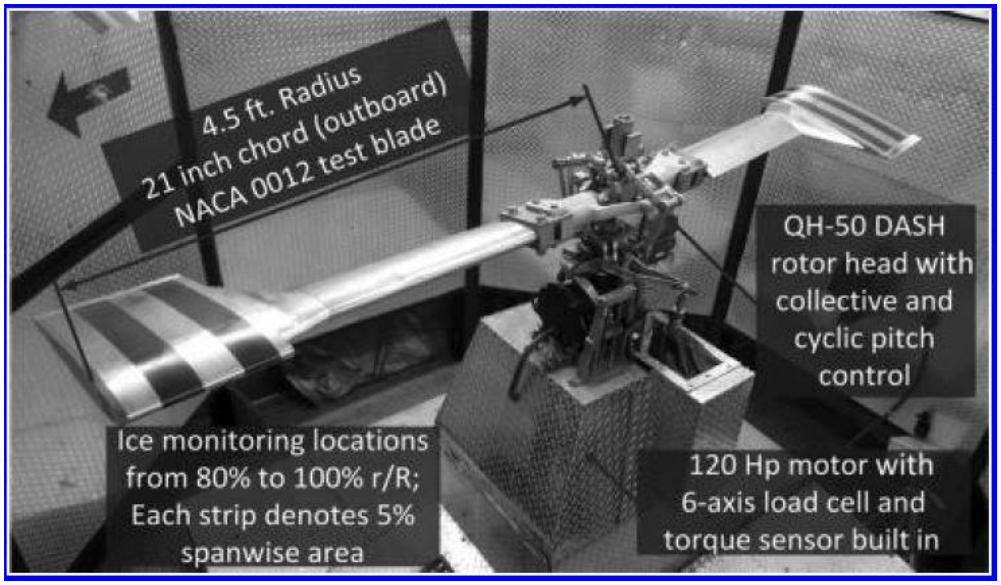

Fig. 3.3 AERTS rotor-icing-test stand with the test blade mounted [18]

3.4.2 Ice Accretion model validation

Using the ice accretion models discussed previously, following two experimental conditions are considered for ice accretion calculations over NACA 0012 airfoil as shown in table 3.1.

Table 3.1 Icing conditions for the ice-shape models

Model number	Temperature (°C)	Velocity (m/s)	MVD (μm)	LWC, (gm/m^3)	Icing time (Min)	AoA (Deg)
Condition 1	-9.7	58.1	20	2.1	5	0
Condition 2	-13.3	67.1	20	1	6	4

For the above icing conditions the ice shapes are reproduced using the numerical models and compared with experimental icing profile and presented in fig 3.4 and 3.5. The computed and experimental ice shapes are found to be in good agreement in most of the iced region except some (17-20%) variations at about 10-15% location away from the stagnation point. Further the calculated ice shape could not produce the rough crests and troughs as in case of experimental results. However the general ice shapes and stagnation-line ice thickness of calculated ice profile are found to be in good agreement with experimental values.

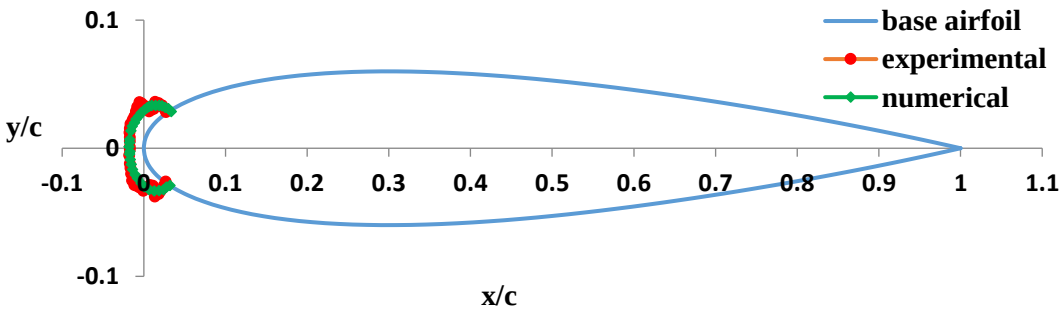

Fig. 3.4 Ice-shape for condition 1 comparison with the reference literature

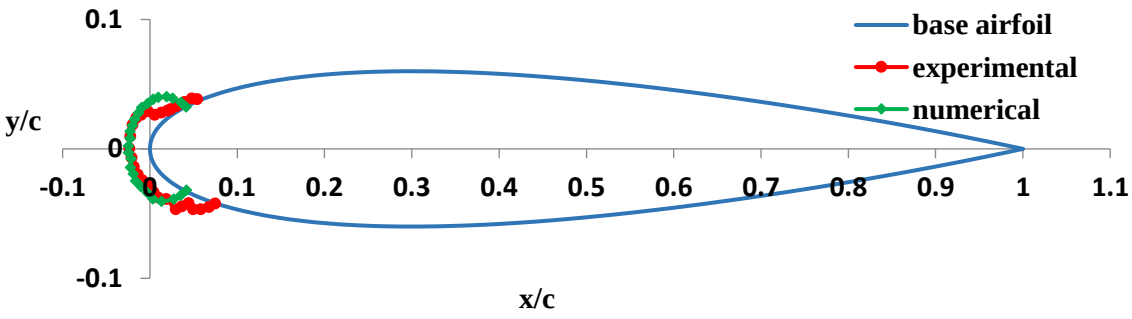

Fig. 3.5 Ice-shape for condition 2 comparison with the reference literature

The differences in the stagnation line thickness for the two ice cases are within 3-7% which is shown with respect to experimental results in table 3.2.

Table. 3.2 Ice-shapes comparison with the reference literature

Ice models	Condition 1	Condition 2
Experimental stagnation line ice thickness (m)	0.017306	0.023608
Numerical stagnation line ice thickness(m)	0.018391	0.02452
% difference	6.26%	3.89%

3.4.3 Aerodynamic validation

Han and Palacios [18] had extended their study to evaluate the degradation of aerodynamic performance of iced blades by creating Poly Urythrene casting exactly matching with the iced shapes over the leading edge of the blades. The wind tunnel results predicted the variation of coefficient of lift and drag versus angle of attack. The airfoil had two parts: removable leading-edge ice-shape-casting models and a trailing-edge base. The two ice-shape-casting models were mounted to the trailing-edge base. The wind tunnel test section with replica of ice-accreted airfoil mounted in the wind tunnel is shown in fig. 3.6. During the test, the test speed was measured to be 40 m⁄s. The corresponding Reynolds number was on the order of 1.4×10^6.

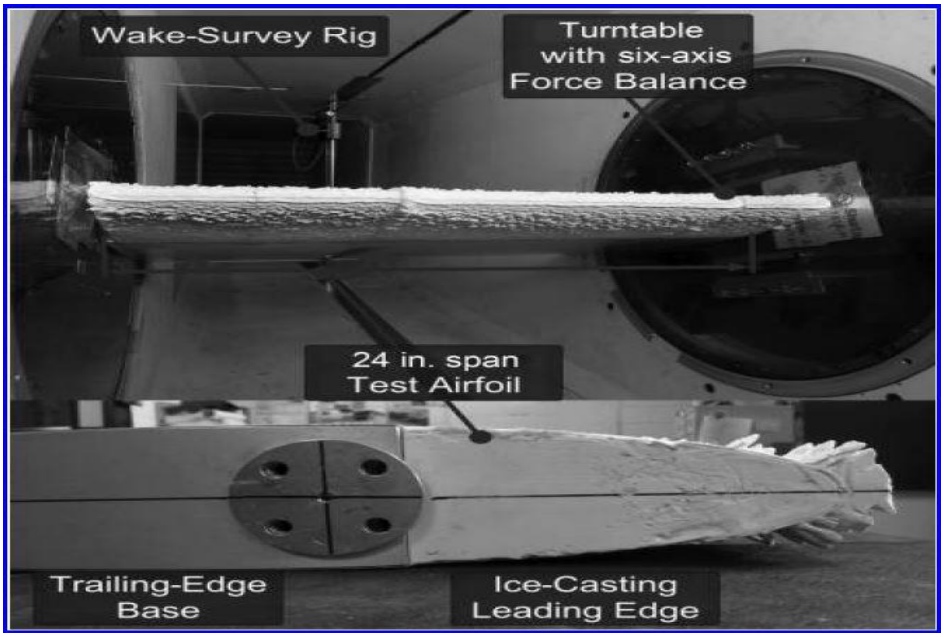

Fig. 3.6 Wind-tunnel test section with airfoil mounted [18].

3.4.4 Computational set-up

Since in the experimental set up the blade covered entire width of the wind tunnel, the flow in the wind tunnel can be considered as 2-D flow. Therefore, the geometry for the CFD computation is generated in 2-D with C-domain. The domain is extended to 12.5C (where C=0.5334 m is chord length of airfoil) from leading edge and top surface of airfoil and 25C from trailing edge to capture any flow structures in the vicinity and away from airfoil. The domain is discretized using unstructured grid with a total of 96,247 cells with minimum and maximum cell sizes 0.00657 and 0.50. The domain, overall mesh and close-up mesh used for CFD study are presented in fig 3.7, 3.8, 3.9 and 3.10 respectively below.

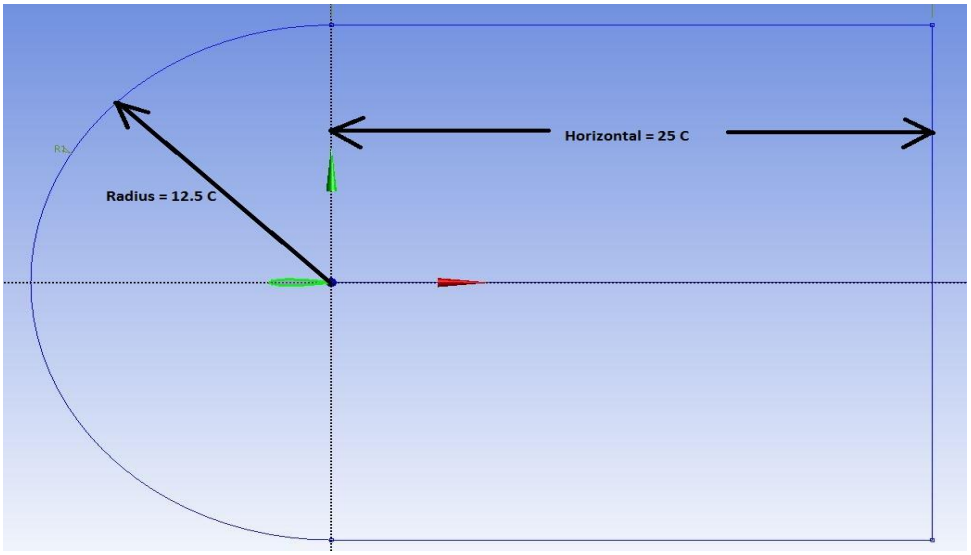

Fig. 3.7 Selection of domain

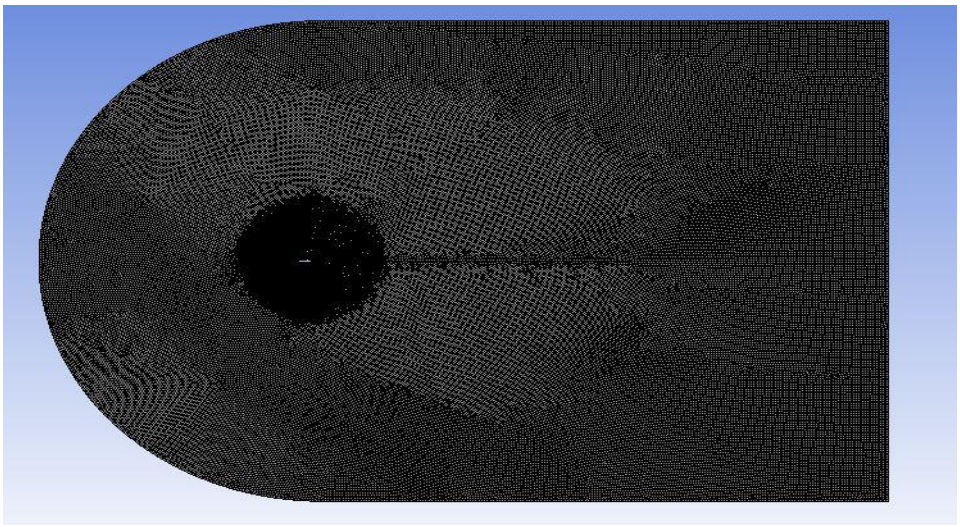

Fig. 3.8 Unstructured mesh

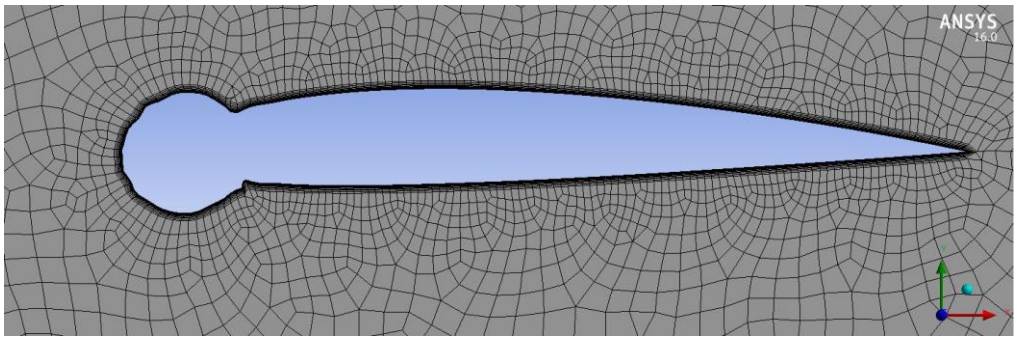

Fig. 3.9 Inflation layers around the edges

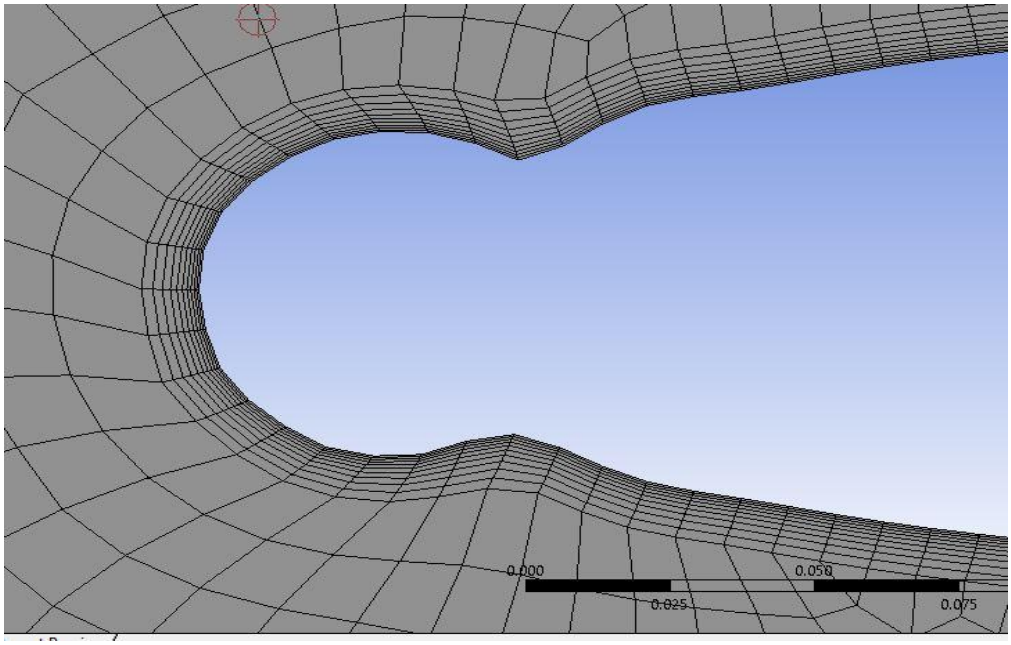

Fig. 3.10 Close up view of the inflation layers around the edges

3.4.5 Boundary conditions

The boundary conditions applied to flow domain are as shown in fig 3.11. The inlet boundary is defined as velocity inlet condition with free stream velocity. The angle of attack is changed by specifying the x component and y-component velocity. The top and bottom extents of domain are also assigned with velocity inlet boundary conditions. This is exactly the same as inlet boundary condition. The airfoil and any ice accreted over the leading edge of airfoil is assumed as wall boundary condition where no-slip boundary is specified. The outlet is assigned with pressure outlet boundary condition, where the pressure of any back flow is specified.

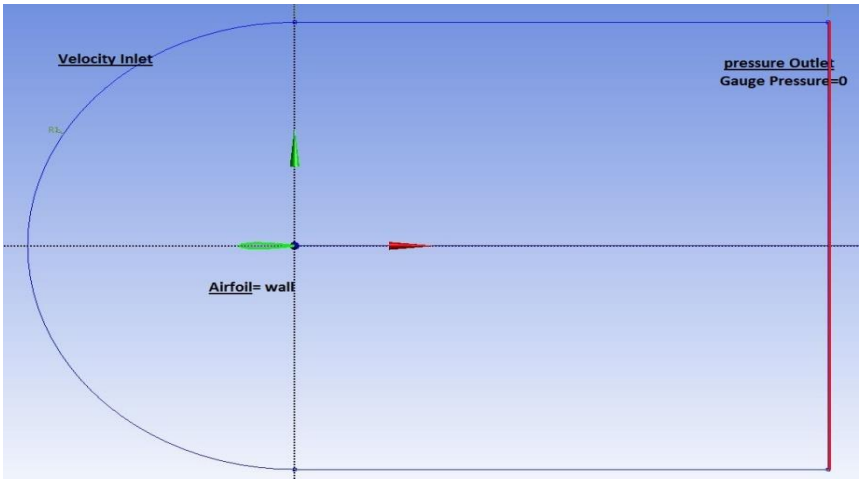

Fig 3.11 Boundary conditions

In order to validate the CFD computations, the wind tunnel experimental aerodynamic data (coefficient of lift and coefficient of drag versus angle of attack) of the Pennsylvania State University was compared with the numerically computed ice shape aerodynamic data. While undertaking the CFD simulation, the selection of mesh is applied with the boundary conditions as specified in section 3.4.4 and 3.4.5.

The coefficients of lift for the iced airfoil found by the experiment to those produced by the ANSYS simulations for the ice shape of condition 1 are compared. And the comparison showed reasonably low percent differences. While comparing with the performance of the base airfoil the for the same AoA the ice accreted airfoil for both experimental and simulated ice shape have shown a decrease in coefficient of lift and a relatively small stall angle. The experimental case have shown a maximum 36% decrease in lift at a stall angle of about 16 deg while for the simulated data it was 34.7% at the same angle of attack. This close convergence of the simulated data with the experimental one proves the validity of the numerical model used in this study.

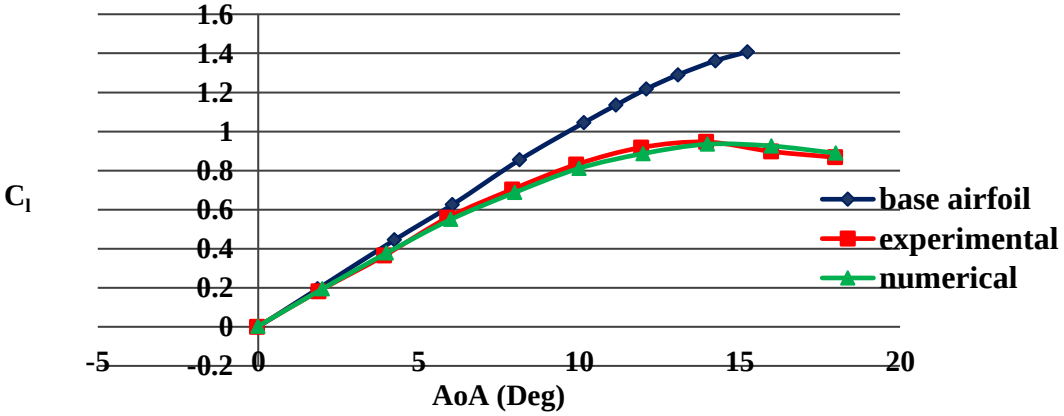

Fig. 3.12 Comparison of coefficient of Lift

To expand the current study, coefficient of drag for a full range of AoA for the ice shape of condition 2 is compared with the experimental data from the reference literature. As it can be seen from fig. 3.13 that the graphs behaves very similarly for the low AoA. As at the low AoA, no separation or very little separation of flow occurred. And the comparison shows 90.21 % increase in drag at an angle of attack of 12 deg for the experimental data while the increase was 89.81% for the same AoA for the computational case. Such closeness of the two results proves the validity of the numerical model used in the current study.

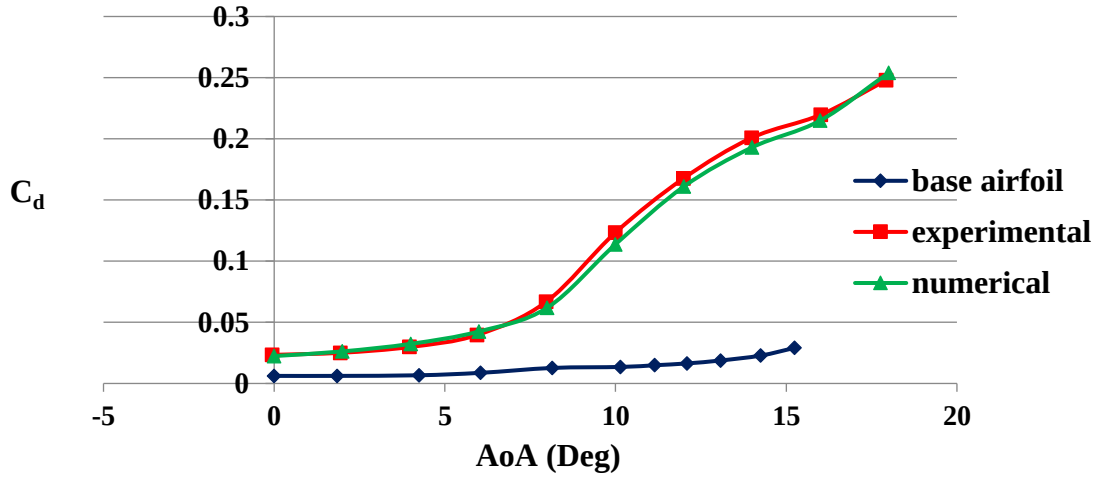

Fig 3.13 Comparison of coefficient of drag

3.5 Mesh Validation

To investigate how computational results vary as mesh quality increases, 5 different grid numbers were considered to obtain coefficient of lift for a full range of angle of attack.

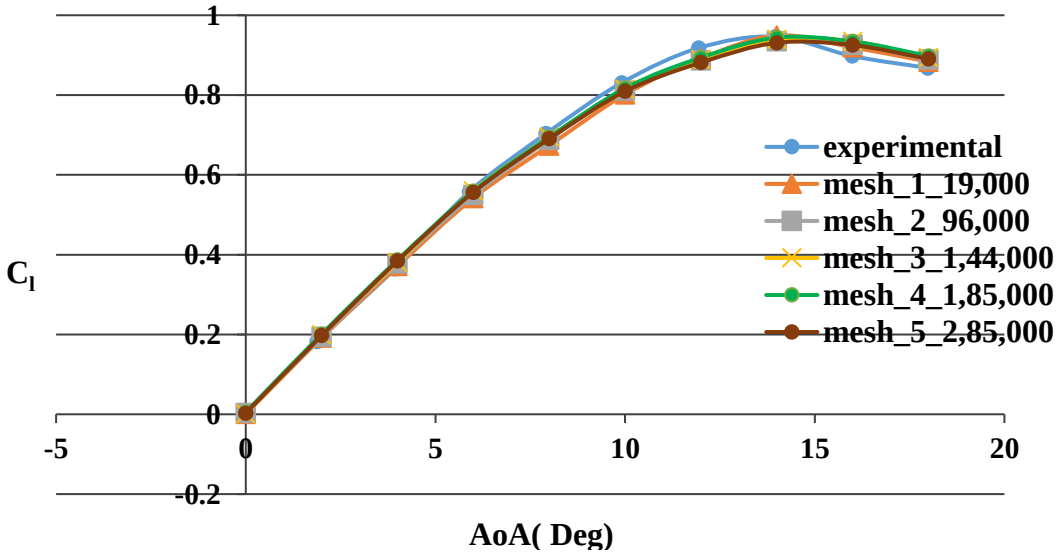

Fig. 3.14 Mesh validation

As can be seen in fig. 3.14, when the mesh quality is increased, the computationally simulated coefficient of lift appears to converge and is almost close to the experimental value for all of the grid sizes. At an AoA of 16 deg, the minimum difference with the experimental results is 3.09% for the mesh quality 2 (96,000 nodes) and 3.035% for the mesh quality 5 (mesh grids 2,85,000). The same is true with the coefficient of drag. In effect, any of these two grids can be used for the above numerical model. So considering the computational time the mesh quality 2 (grid number= 96,000) is used throughout the whole study.

CHAPTER 4

PROBLEM SPECIFICATION AND SOLUTION

4.1 Overview

Chapter 4 discusses the specification of the problem and solution of the problem using the numerical model developed in this study. This chapter also describes the effects of each parameter and meteorological conditions on ice formation in order to determine the worst icing cases. These parameters include aircraft geometry, collection efficiency, freezing fraction, aircraft surface temperature, free- stream velocity and time of ice accretion. Moreover, in order to determine the severity of icing it is necessary to study the meteorological conditions like liquid water content, droplet size and outside surface temperature in relation to the aircraft operating conditions for different flight paths. The aerodynamic performance degradation of the iced airfoil with respect to the base airfoil was also analyzed.

4.2 Problem Specification and Formulation

4.2.1 Problem specification

The main subject matter of the study is the in- flight ice accretion phenomena around an asymmetric airfoil and analysis of the aerodynamic performance of the degraded airfoil profile depending upon the flight conditions, airfoil geometry and ambient weather conditions.

4.2.2 Problem formulation

Prediction of the ice accumulation over NACA 2412 airfoil and aerodynamic performance investigation under inclement weather conditions requires a deep understanding of the physics of the problem.

In flight icing is the condition when air containing liquid water droplets strikes a cold surface having temperature below freezing point. Depending upon the weather conditions, in- flight icing may be of various forms and may form for a different duration of time. As mentioned earlier in the literature, icing is mainly classified as glaze or clear ice, rime ice, mixed ice and frost. Hence icing will have different derogation effects on the airfoil aerodynamics. So it is the prime concern of the present study and one of the most sensitive problems encountered by the aviation industry when the aircraft is flying within

altitude range of 3000m to 8000m(10,000 ft to 25,000 ft), where air temperature is -10°C to -40°C.

4.3 Methodology

4.3.1 Numerical Model for leading edge ice accretion

The basics of ice formation can be formulated in terms of geometric parameters and ambient conditions to calculate the stagnation point as well as the general ice thickness. The solution includes calculation of catch rate or collection efficiency based on Langmuir and Blodgett Trajectory Model and mass inflow of water using Impingement Model and finally to calculate the ice thickness using Ice Growth Model at each point of interest on the airfoil surface. All these values are estimated based on the governing parameters.

4.3.2 Assumptions

To simplify the problem and ease of calculation the following assumptions are made:

i. The aircraft is flying at level flight within icing clouds, hence all calculation of ice thickness is done at zero degree angle of attack.

ii. The freezing point of water and melting point of ice is the same.

iii. The aircraft surface or skin temperature is at freezing temperature for icing to be occurred.

iv. The analytical freezing fraction value ranges from 0.3 to 1.0 from Messinger's Heat Balance Analysis for effective ice accretion.

v. Air flow around the airfoil surface is considered to be turbulent and compressible.

vi. Ice accretion is considered for an airfoil of a high performance subsonic aircraft.

4.3.3 Parametric analysis of icing parameters

As a way of determining the influence of the above mentioned and other relevant parameters on ice accretion some reference cases are made and each parameter has been changed while maintaining the others. The selection of these parameters are made for an airfoil of NACA 2412 of 1m chord length through different forms of clouds, based on the standards established from experimental data and literature on aircraft icing.

Case I: A high performance, subsonic aircraft with an airspeed of 122 m/s (Re = 6×10^6) is considered to be at level flight within an altitude range of 12,700 ft (3898m approx.) through medium level Nimbostratus clouds [41]. Air at this altitude has a low

amount of Liquid Water Content, low catch rate but high accumulation rate as the air temperature is within -10°C. Other ambient conditions are listed below according to the standard atmosphere chart (SI units):

Table. 4.1 Ambient conditions for case I

Parameters	**Numerical values**
Altitude (h)	3,898 m
Temperature (T)	-10°C or 263.15 K
Ambient pressure (P)	$6.246\times 10^{4}\ N/m^2$
Density of air (ρ_{air})	.828 Kg/m^3
Dynamic viscosity (μ)	$1.69\times 10^{-5}\ Kg/ms$
Liquid Water Content (LWC)	.81 gm/m^3
Density of ice (ρ_{ice})	919.2 Kg/m^3
Free stream velocity (V)	122 m/s
Reynolds number (Re)	6×10^{6}

As stratus clouds have extensive horizontal coverage to over several thousand feet but small vertical coverage of mostly 3000 ft [42], the flight within nimbostratus clouds at level flight will be affected by long duration of icing resulting in rime ice formation. Considering a nimbostratus clouds with horizontal coverage of 10 to 15NM, the aircraft with velocity 122 m/s is supposed to be within icing clouds for a duration of 227 s (15NM/ 122m/s) in an average. So based on the flight conditions mentioned in table. 4.1 icing calculation is done for the following time duration and analytical freezing fraction values:

Table. 4.2 Icing duration and intensity case I

Freezing fraction	**Time of ice accretion**
0.3	600s
0.5	300s
0.7	120s, 600s
1.00	120s, 300s, 600s

Case II: The very particular aircraft is again considered to be in level flight within an altitude of 17,000ft (5395 m approx) with an higher airspeed of about 142 m/s (Re=

6×10^6). The Reynolds number was considered constant for observing the effects of other parameters. At this altitude medium level altocumulus clouds exist which have with high concentration of SLD (Super cooled Liquid Droplets), higher catch rate and high LWC. This causes the worst icing case but for a short duration as cumulus clouds have limited horizontal coverage but extended vertical coverage of several thousand feet. Other ambient conditions at this altitude are listed in the following table:

Table. 4.3 Ambient conditions for case II

Parameters	**Numerical values**
Altitude (h)	5,395 m
Temperature (T)	-20°C or 253.15 K
Ambient pressure (P)	$5.1226 \times 10^4\ N/m^2$
Density of air (ρ_{air})	.70513 Kg/m^3
Dynamic viscosity (μ)	$1.67\times 10^{-5}\ Kg/ms$
Liquid Water Content (LWC)	1.193 gm/m^3
Density of ice (ρ_{ice})	919.4 Kg/m^3
Free stream velocity (V)	142 m/s
Reynolds number (Re)	6×10^6

As a single cumulus cell extend for a horizontal range of 2 NM to maximum 6 NM [42], with an airspeed of 142 m/s the aircraft is supposed to be within icing cloud for a duration of 80s (6NM/142 m/s) on an average. So, icing duration will be longer if the aircraft is to fly through a number of cumulus cells contributing to the most critical icing conditions. So ice prediction time is considered as per the following table and freezing fraction values:

Table. 4.4 Icing duration and intensity case II

Freezing fraction	**Time of ice accretion**
0.3	700s
0.5	500s
0.7	300s, 700s
1.00	80s, 300s, 700s

Case III: If the aircraft is considered to fly at a higher altitude range of 22,000 ft (about 8000 m) where the air temperature is within -30°C to -40°C and icing threat is present due to the presence of cirrocumulus clouds (20,000 ft to 40,000 ft) containing high LWC and high catch rate. As cirrocumuls clouds are formed entirely from ice and super cooled water icing at this cloud is severe in intensity contributing to the glaze ice or clear ice. According to the standard altitude chart other ambient conditions are enlisted in the following table.

Table. 4.5 Ambient conditions for case III

Parameters	**Numerical values**
Altitude (h)	6,893 m
Temperature (T)	-30°C or 243.15 K
Ambient pressure (P)	4.1666× 10^4 N/m^2
Density of air (ρ_{air})	.596 Kg/m^3
Dynamic viscosity (μ)	1.66× 10^{-5} Kg/ms
Liquid Water Content (LWC)	1.131 gm/m^3
Density of ice (ρ_{ice})	919.6 Kg/m^3
Free stream velocity (V)	167 m/s
Reynolds number (Re)	6× 10^6

As cumulus clouds usually have limited horizontal coverage (a single cumulus cell is extended up to 2NM to 6NM), it covers a small duration of the flight time. So, based on the above situation, icing time can be 56s (6NM/ 167m/s) to more. Hence, ice accretion prediction was made for the following freezing fractions and time durations of table 4.6.

Table. 4.6 Icing duration and intensity case III

Freezing fraction	**Time of ice accretion**
0.3	500s
0.5	200s
0.7	200s, 500s
1.00	50s, 200s, 500s

4.3.3.1 Reynolds number variation

Aerodynamic coefficients for base airfoil are influenced by the variation in Reynolds number. So the variation can be valid for the ice accreted airfoil shape also. Therefore, in

order to investigate the influence of Reynolds Number, CFD analysis is undertaken for Re=5× 10^6 , 8× 10^6 and 15× 10^6 for same ambient conditions of table 4.3.

4.4 Results and Discussion

In this section the ice prediction results from the numerical model and the aerodynamic performance simulation from the computational model for the worst possible flow cases are presented.

4.4.1 Ice accretion

Applying the developed numerical model ice accretion over NACA 2412 airfoil for the above discussed cases forty two ice tracings are calculated and general ice shapes are produced around the airfoil using numerical computational tool MATLAB 14.0. The worst cases of calculated leading edge ice thickness values for the above conditions are enlisted in the following table.

Table. 4.7 Stagnation point ice thickness

Ice case	Freezing fraction (f)	Time of ice accretion (s)	Ice thickness at stagnation point ,h_{ice} (m)
Case I	1	600	.0642
Case II	1	700	.1282
Case III	1	500	.1022
Case IV Re= 5× 10^6	1	700	.1067
Case V Re = 8× 10^6	1	700	.1202
Case VI Re = 15× 10^6	1	700	.1458

Ice tracings for the above worst icing cases are presented below:

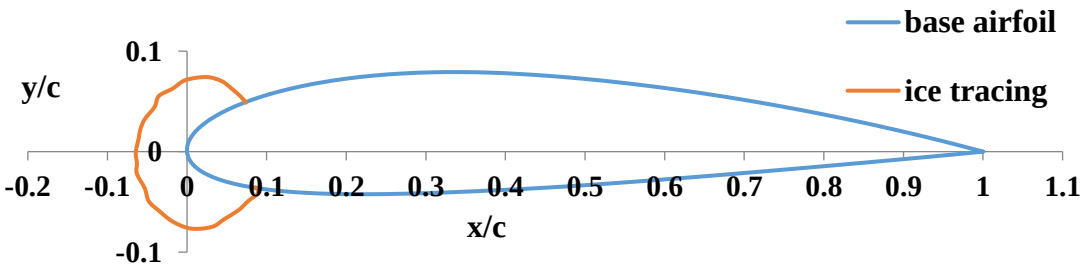

Fig. 4.1 Ice shape for case I((Re= 6× 10^6)

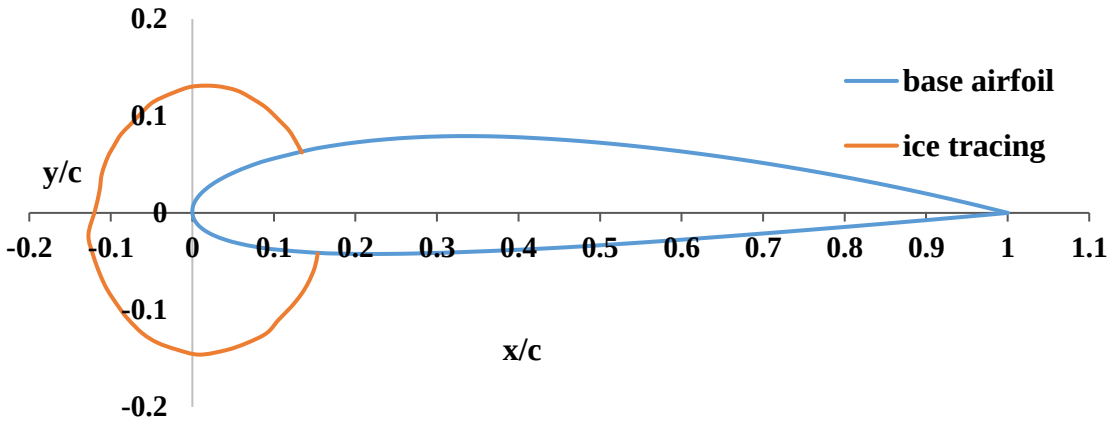

Fig. 4.2 Ice shape for case II (Re= 6× 10^6)

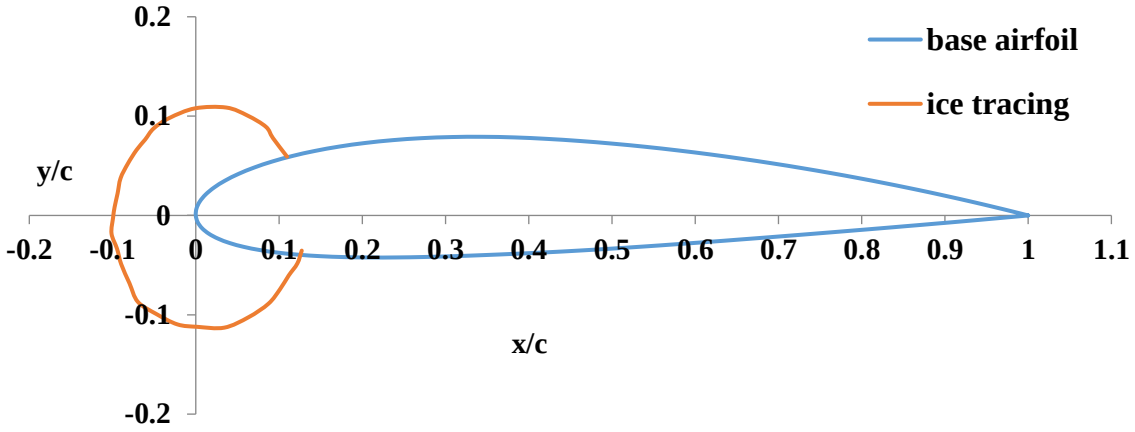

Fig. 4.3 Ice shape for case III (Re= 6× 10^6)

Sample ice tracings are produced for the above three cases for different ambient conditions at different altitude but at the same Reynolds number. The analytical freezing fraction value is varied from 0.3 to 1. The results show the worst icing cases in term of maximum thickness at the stagnation point for freezing fraction value 1 for each of the cases. Though the free-stream velocity is maximum for case III (167m/s), case II generated the maximum icing as the time of ice accretion was maximum (700s). Hence the above ice tracings show a significant influence of the time of ice accretion on ice thickness over the airfoil surface. And the results give a maximum ice thickness of 0.1282 m at the stagnation point for case II generating mixed ice characteristics. Therefore, the ambient conditions like density of air, density of water, viscosity of air might have very small influence over ice accretion at the same Reynolds number.

4.4.1.1 Effects of Reynolds number variation

In order to see the influence of variation of Reynolds number following ice tracings are produced with the above mentioned Reynolds number for the same ambient conditions of table 4.3.

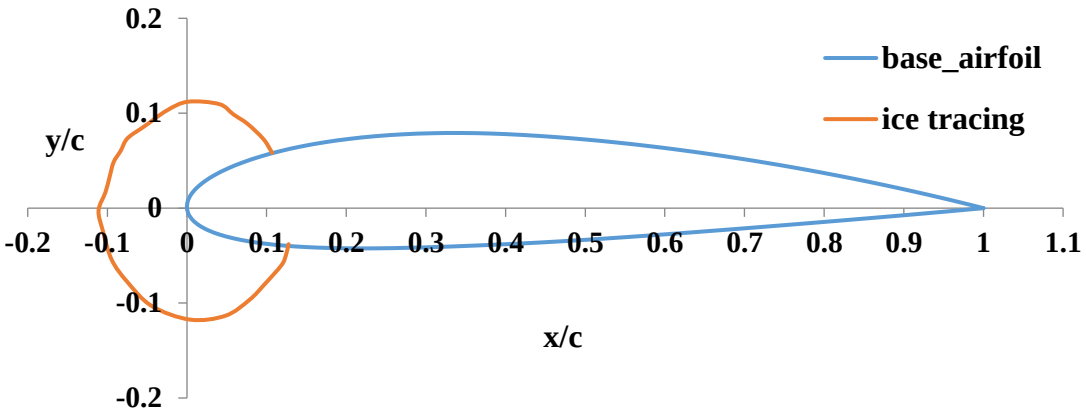

Fig. 4.4 Ice shape for case IV (Re= 5×10^{6})

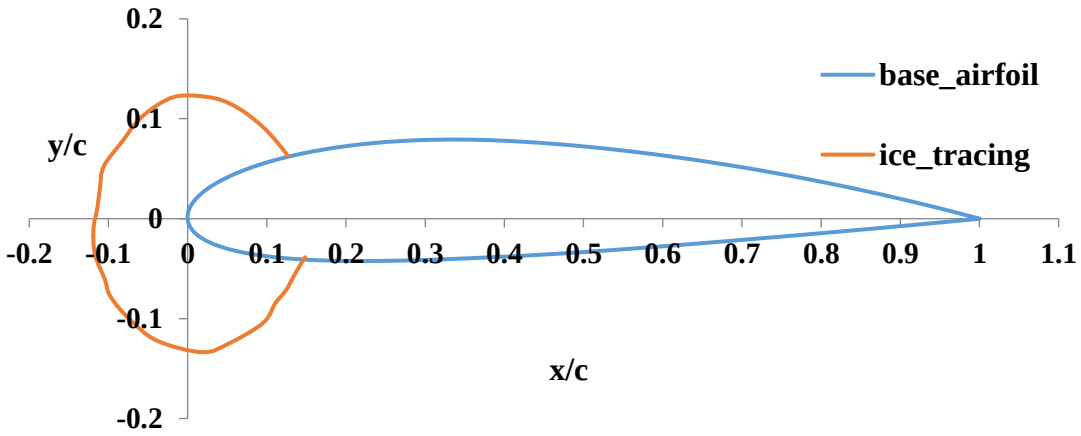

Fig. 4.5 Ice shape for case V (Re= 8×10^{6})

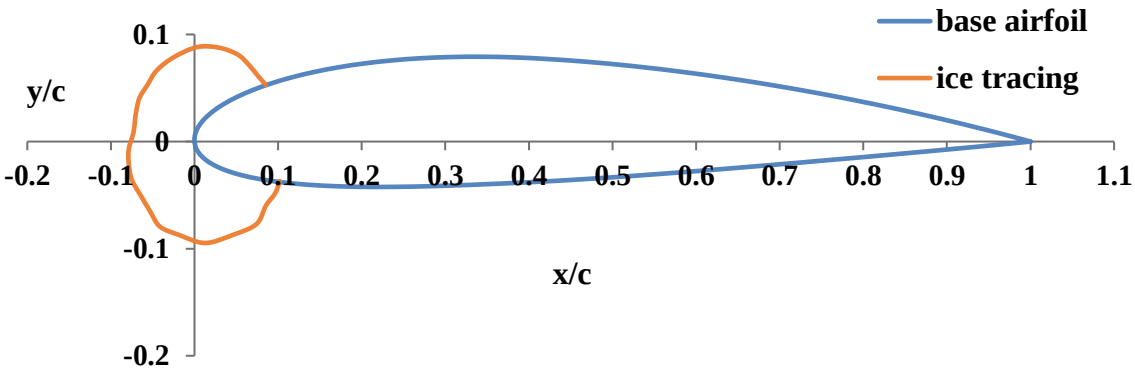

Fig. 4.6 Ice shape for case VI (Re= 15×10^{6})

The above three ice tracings show an effect of Reynolds number variation. Calculated ice shapes show a maximum ice thickness of 0.1458 m at the stagnation point for the maximum Reynolds number of 15×10^{6} .

4.4.2 Aerodynamic performance analysis

CFD analysis of the clean and iced airfoils for the above cases is done using the k-ε turbulent model using the similar domain, boundary conditions and grid discussed previously in chapter 3. The aerodynamic performance of iced airfoil is compared with the base airfoil in terms of the coefficient of lift and coefficient of drag and the following results are found.

Case I:

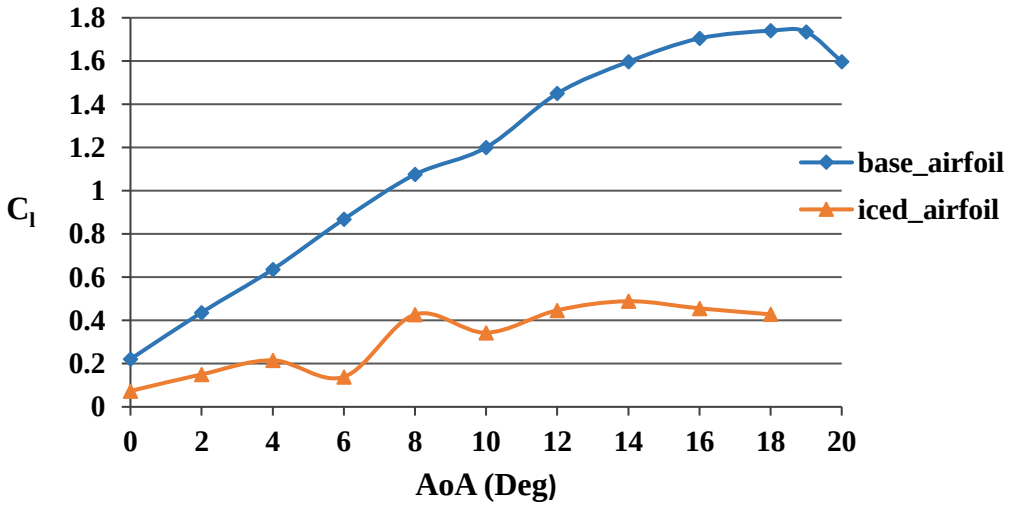

Fig. 4.7 Angle of attack vs Coefficient of lift (Re= 6×10^6)

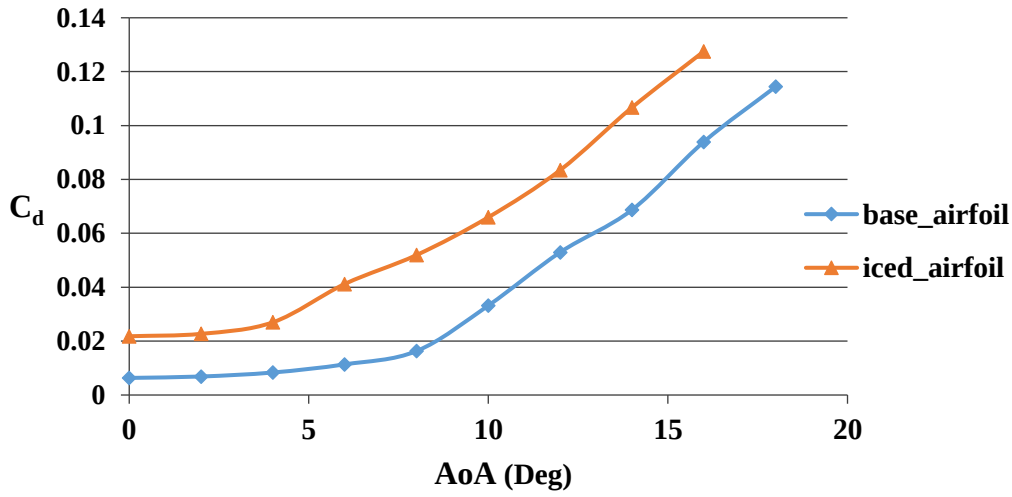

Fig. 4.8 Angle of attack vs Coefficient of drag (Re= 6×10^6)

From the above plot for case I, the iced airfoil shows a maximum 84.02% decrease in lift coefficient and 262% increase in drag coefficient at 6 degree angle of attack compared to the base airfoil. And the maximum difference in ice thickness is 20% between upper and lower surface. The average increase in drag coefficient for the iced airfoil is 158.28% compared to the base airfoil.

The lift curve shows a fall in coefficient of lift at 6° AoA, again a rise at 8° AoA and a fall at 10° AoA and then an almost constant coefficient of lift beyond 10° AoA. Such aerodynamic performance degradation of the iced airfoil can be explained from fig. 4.9 to 4.12 observing the velocity vector which is colored according to velocity magnitude. This phenomenon compiles with the Bernoulli's equation.

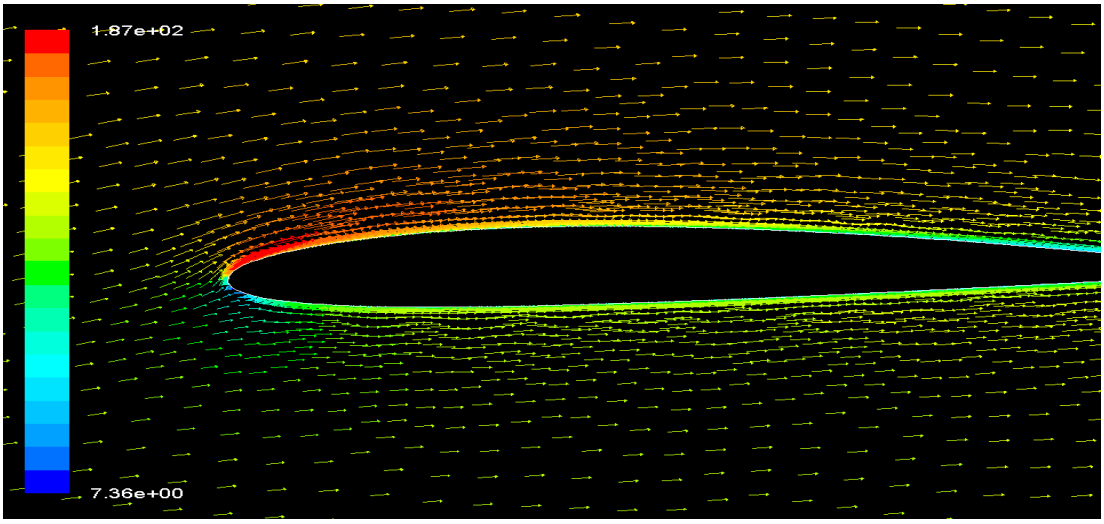

Fig. 4.9 Velocity vector for base airfoil at 6° AoA

The velocity vector of fig 4.9 for base airfoil shows still attached flow at 6° AoA generating more lift than drag. But the velocity vector of fig. 4.10 for the iced airfoil at 6° AoA shows a reverse flow at the ice accreted surface for both upper and lower surfaces causing the velocity to reach almost zero at the boundary layers. This reverse flow resulted in a very low lift coefficient and higher drag coefficient compared to the base airfoil. This indicates that the airfoil approaches to stall condition at only 6° AoA.

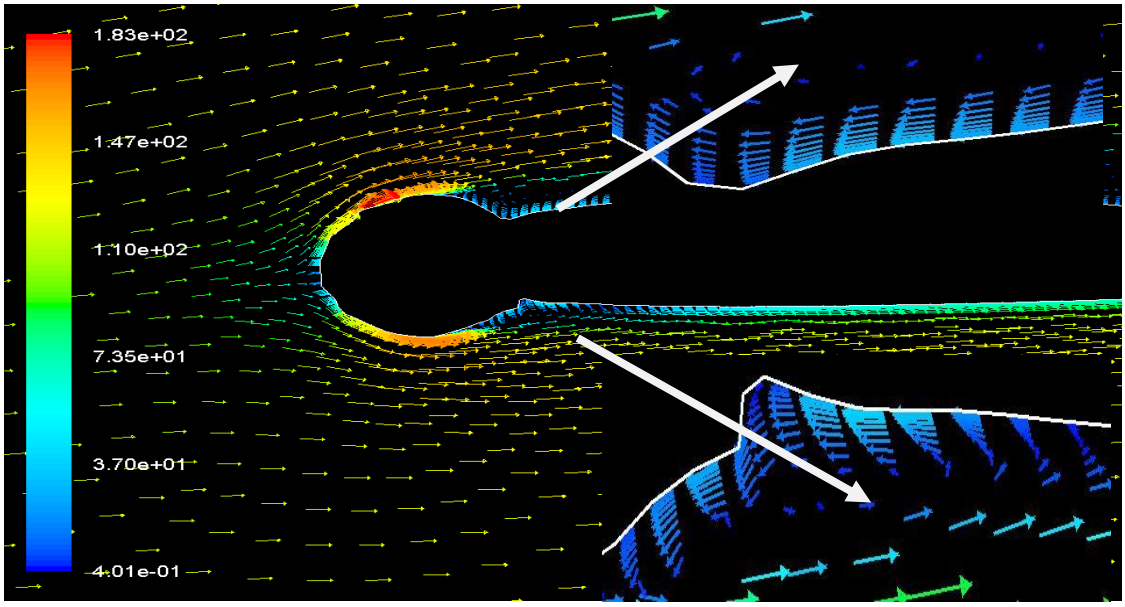

Fig. 4.10 Velocity vector for iced airfoil at 6° AoA

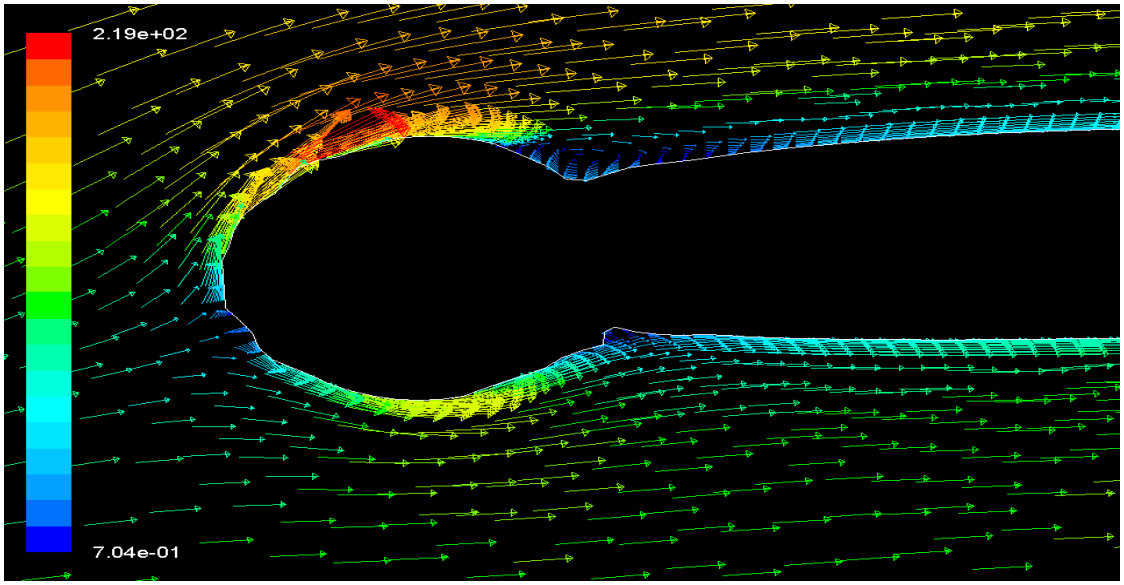

Fig. 4.11 Velocity vector for iced airfoil at 8° AoA

However, the lift coefficient again increased at 8° AoA because of flow reattachment and is evident from the fig 4.11. This is because of the fact that air accelerates on the upper surface, as marked by an increase in velocity magnitude.

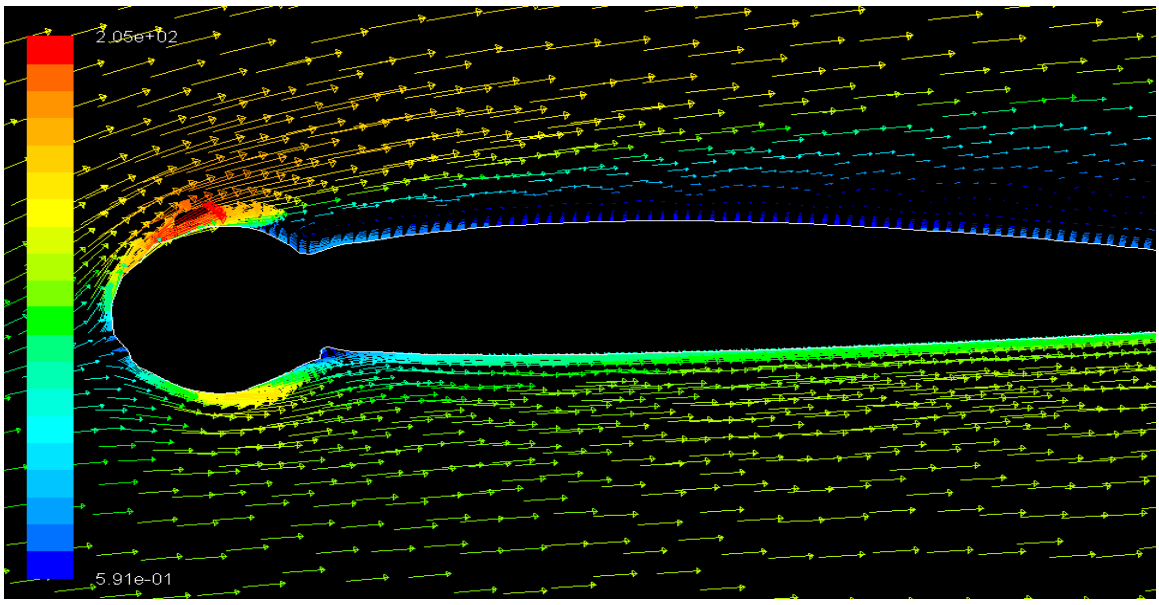

Fig. 4.12 Velocity vector for iced airfoil at 10° AoA

Beyond 8° AoA the coefficient of lift decreases and the coefficient of drag remains constantly increasing because of the flow separation at the upper surface of the airfoil section as seen in fig. 4.12.

Case II:

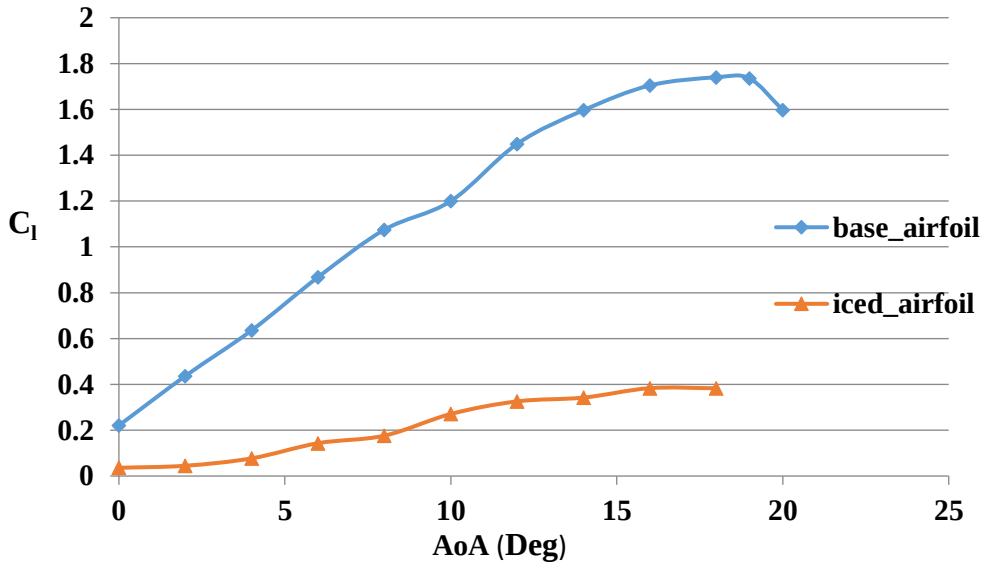

Fig. 4.13 Angle of attack vs Coefficient of lift (Re= 6× 10^6)

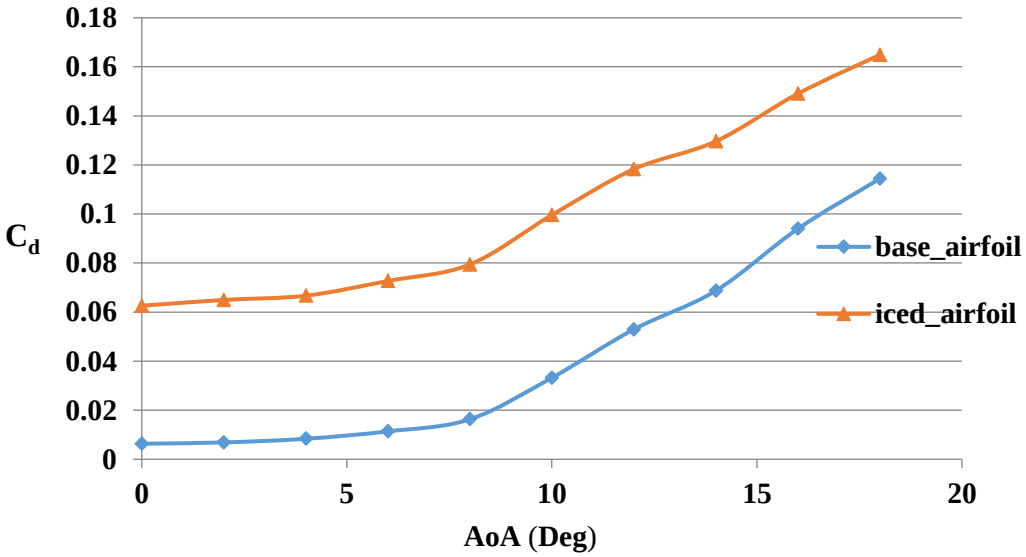

Fig. 4.14 Angle of attack vs Coefficient of drag (Re= 6× 10^6)

Investigating the aerodynamic performance of the iced airfoil for case II gives a maximum 89.713% reduction in lift coefficient at 2 deg angle of attack and 844% increase in drag coefficient. While at 6° AoA, the reduction in lift is 83.06% and increase in drag coefficient was 538%. At 10° AoA the reduction in lift is 77.42% and increase in drag coefficient was 199.77%. From fig 4.13 and fig. 4.14, stalling occurred beyond 16° AoA and coefficient of drag continued to increase. On an average the coefficient of drag for the iced airfoil increased to 386.95% compared to the base airfoil representing the worst icing case.

Case III:

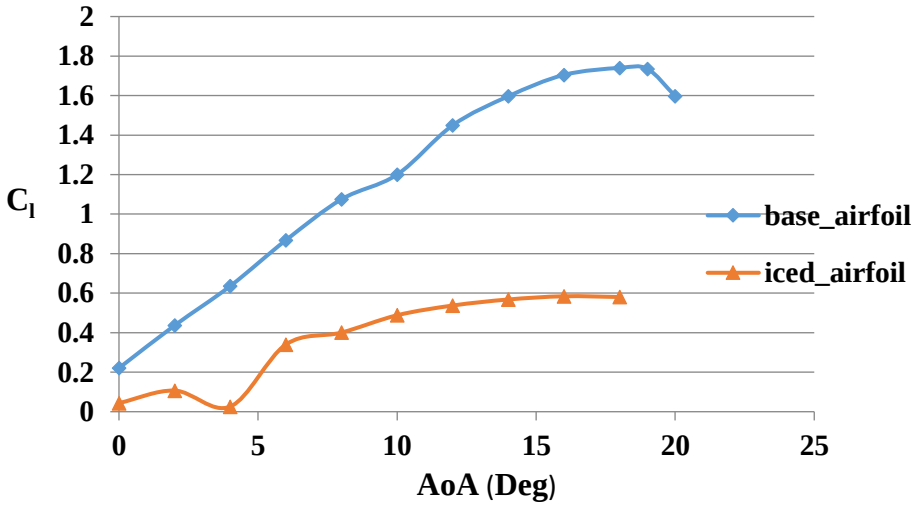

Fig. 4.15 Angle of attack vs Coefficient of lift (Re= 6× 10^6)

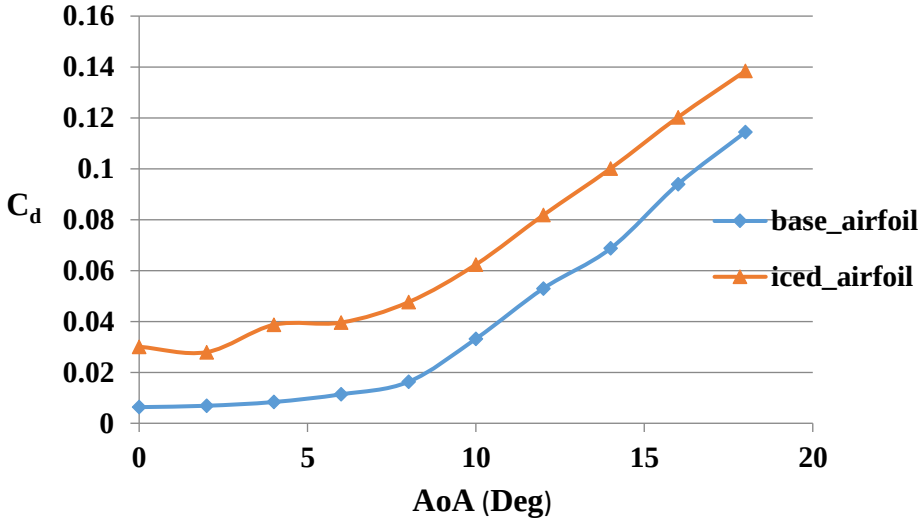

Fig. 4.16 Angle of attack vs Coefficient of drag (Re= 6× 10^6)

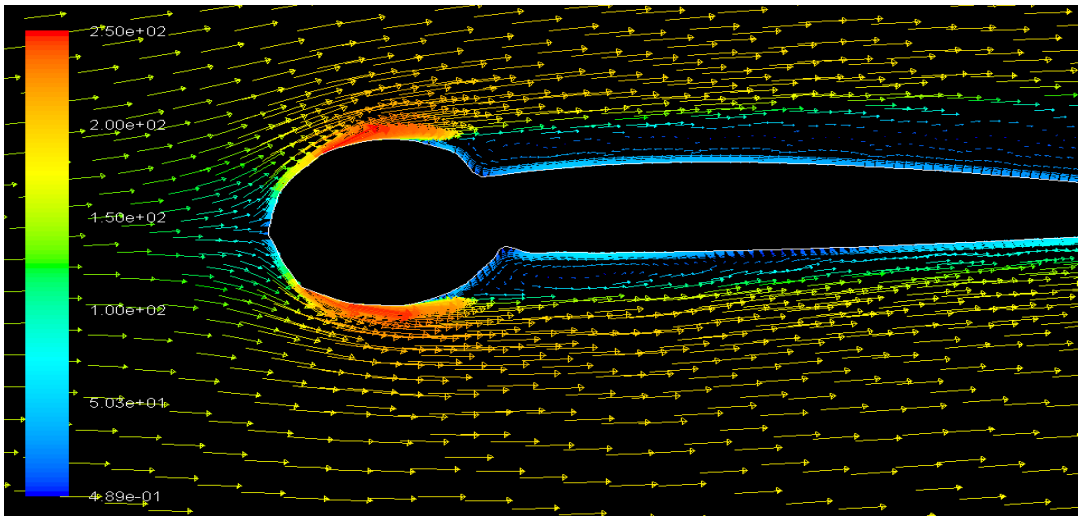

Fig. 4.17 Velocity vector for iced airfoil at 4° AoA

From fig. 4.15 and 4.16, the aerodynamic performance degradation for case III is seen at 4 deg angle of attack with a 95.92% drop in lift coefficient and a 363% increase in drag coefficient. And the average increase in coefficient of drag for the iced airfoil is 172% compared to the base airfoil.

From fig. 4.17, the behavior of iced airfoil shows that the coefficient of lift falls only at 4° AoA as the region of high velocity separates from the airfoil section, giving rise to the stall condition. However, the coefficient of lift for the iced airfoil increased again with angle of attack due to flow reattachment and again falls beyond 16° AoA. But the aerodynamic degradation of the iced airfoil compared to the base airfoil continued to be reducing with the increase in angle of attack.

4.4.2.1 Effects of Reynolds number variation

Case IV: Re= 5×10^6

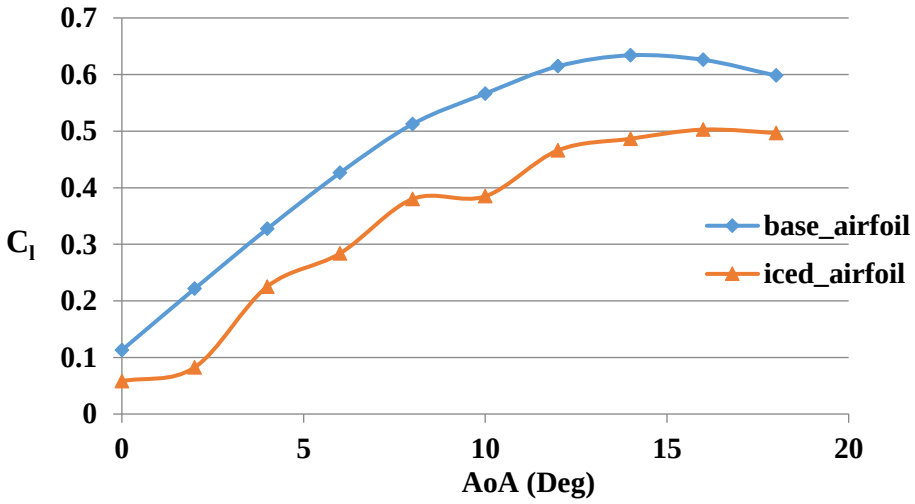

Fig. 4.18 Angle of attack vs Coefficient of lift (Re= 5×10^6)

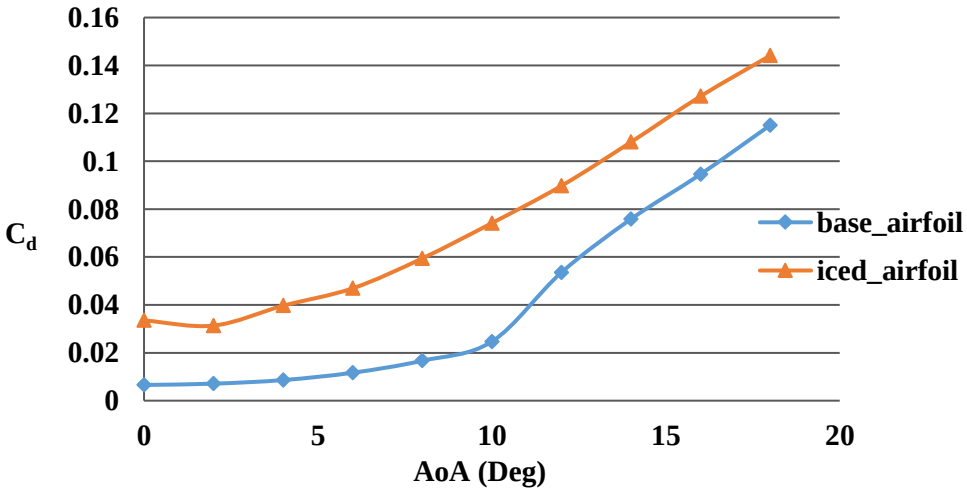

Fig. 4.19 Angle of attack vs Coefficient of drag (Re= 5×10^6)

From fig. 4.18 and 4.19, the maximum drop in coefficient of lift for the iced airfoil is 62.47% that occurs at 2° AoA while increase in drag is 341.74%. The average increase in coefficient of drag for the iced airfoil is 204.25% compared to the base airfoil. However, a degradation in the the values of aerodynamic coefficients for the iced airfoil observed throughout the whole range of angle of attack and finally the airfoil stalls beyond 16° AoA.

Case V: Re= 8× 10^6

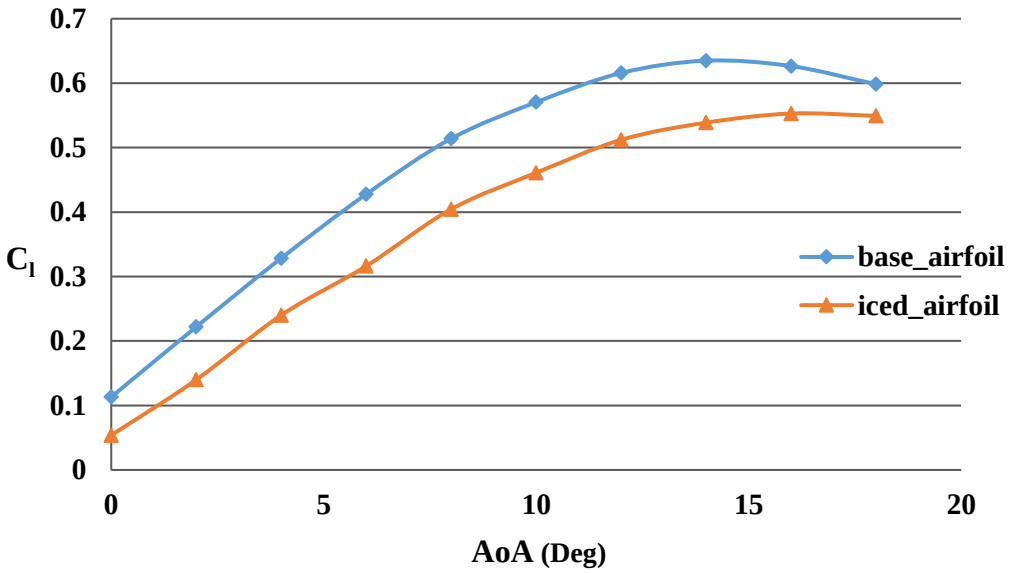

Fig. 4.20 Angle of attack vs Coefficient of lift (Re= 8× 10^6)

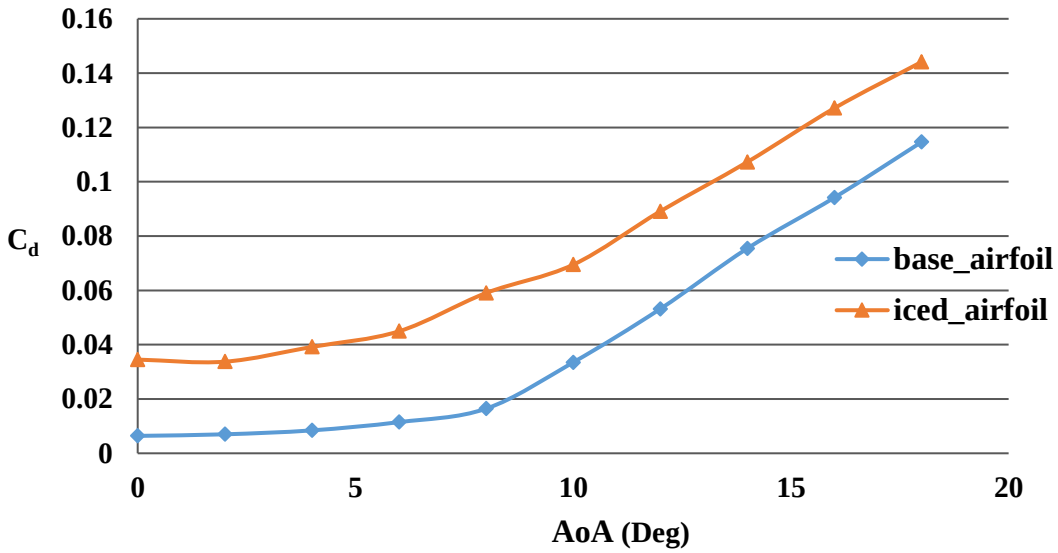

Fig. 4.21 Angle of attack vs Coefficient of drag (Re= 8× 10^6)

The effect of variation of angle of attack on aerodynamic performance for the iced airfoil with increased Reynolds number can be seen from fig. 4.20 and 4.21. As expected from

the NACA 2412 base airfoil, the coefficient of lift is much lower (max 52.44%) and coefficient of drag is higher (max 437.6%) for the iced airfoil. The average increase in coefficient of drag for the iced airfoil is 201.23% compared to the base airfoil. The reason behind this is that the ice shape changes the aerodynamic shape of the airfoil causing reverse flow and thus a very low velocity magnitude at the upper surface. Hence the lift coefficient decreases and drag coefficient increases compared to the base airfoil.

Case VI ((Re= 15× 10^6):

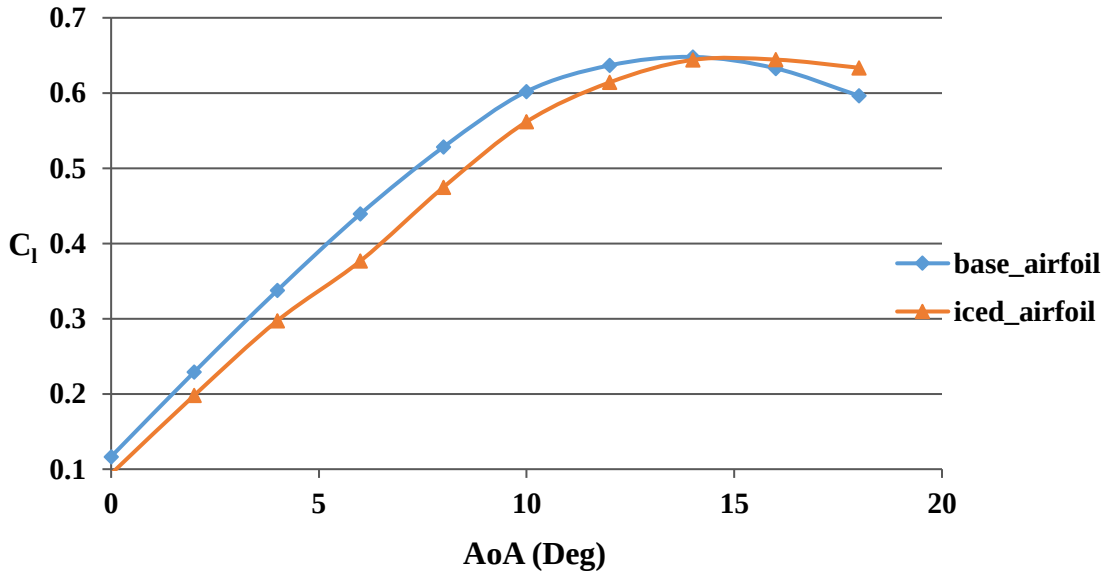

Fig. 4.22 Angle of attack vs Coefficient of lift (Re= 15× 10^6)

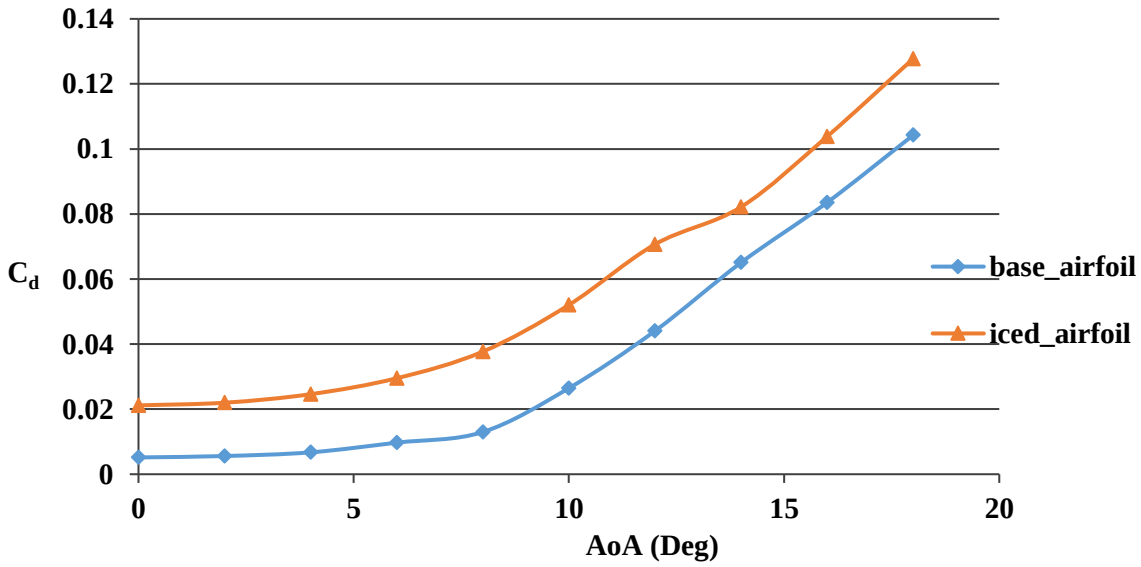

Fig. 4.23 Angle of attack vs Coefficient of drag (Re= 15× 10^6)

From fig. 4.22 and fig. 4.23, at higher Reynolds number (15×10^6), the difference in aerodynamic coefficients of the iced airfoil is relatively low compared to the base airfoil. However, the coefficient of lift remains almost constant beyond 18° AoA but the drag kept increasing for the iced airfoil. Such unusual aerodynamic behavior can be observed from the velocity vector of fig. 4.24.

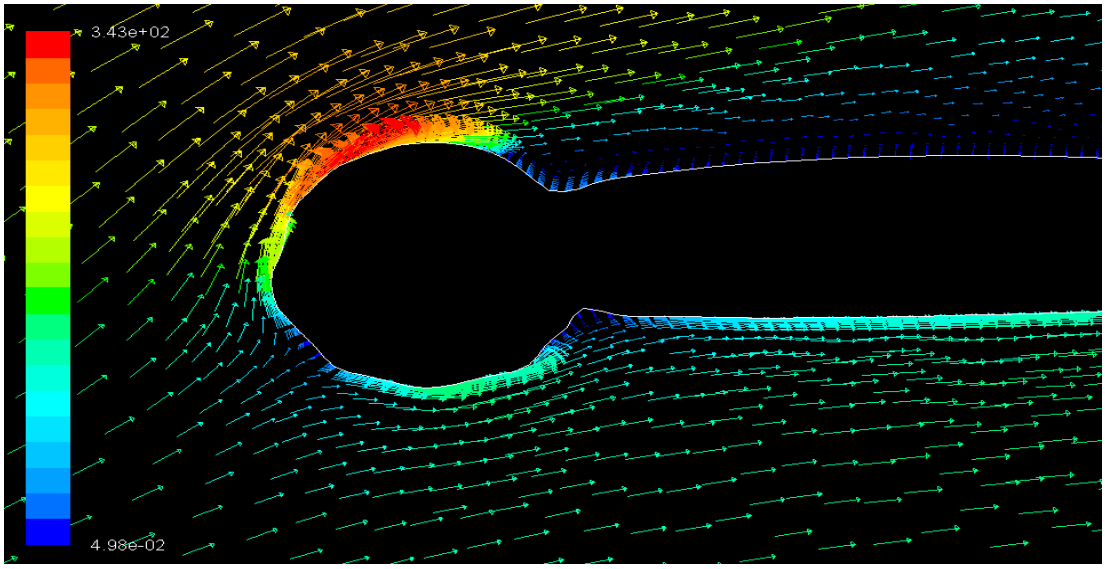

Fig. 4.24 Velocity vector for iced airfoil at 18° AoA

Analyzing the above results is is found that the icing effect on airfoil performance may be minimized when the Reynolds number is increased for the same flight condition. It is also found that there is almost 19% reduction in C_l. The average increase in coefficient of drag for the iced airfoil is 151.28% compared to the base airfoil for Reynolds number of 15×10^6 where, the maximum increase in drag coefficient is 204% for Reynolds number 5×10^6 .

CHAPTER 5

CONCLUSIONS AND RECOMMENDATIONS

5.1 Conclusions

The present work involves development of a computer code to solve thermodynamic and conservation laws for prediction of ice accretion over NACA 2412 airfoil under various flight conditions. The CFD analysis of the ice accreted airfoil is undertaken to assess the variation of aerodynamic coefficients at varying angles of attack. The following conclusions can be drawn from the studies presented in preceding chapters:-

a) Comparison of the ice accreted airfoil shapes for NACA 0012 airfoil with the experimental shape available from open source shows a 6.26% difference for icing case I and 3.895% for icing case II at the stagnation point and also in good agreement at other places which proves the validity of the used numerical model.

b) For case I the maximum difference in ice thickness is 20% between upper and lower surface. So, leading edge ice accretion is more at the lower surface than at the upper surface for a positive cambered asymmetric airfoil NACA 2412 while ice thickness is almost the same for both surfaces for symmetric NACA 0012 airfoil.

c) For the same Reynolds number, icing in altocumulus cloud is 50 % more than nimbostratus cloud and 20% more than cirrocumulus cloud at the stagnation point. Hence icing might be most hazardous within altocumulus cloud having maximum amount of liquid water content.

d) Observing the aerodynamic effect of the ice accreted airfoil, icing caused the airfoil to stall at only 2 deg angle of attack for case II with 89.7% reduction in lift coefficient and 844% increase in drag coefficient.

e) Most dangerous and critical consequence of leading edge icing is the increase in drag and for the worst icing case II in this study it is almost 386.95% on an average compared to the base airfoil.

f) Observing the effects of Reynolds number on the aerodynamic performance, it can be concluded that at the same altitude and flight conditions, increasing the Reynolds number three times, the drop in C_l is almost 27% less and increase in C_d is about 340% less compared to the initial Reynolds number.

g) However, once ice is accreted on the airfoil at zero degree angle of attack, it is observed that the icing effect on aerodynamic performance degradation is

minimized by increasing the angle of attack. So increasing angle of attack might minimize the aerodynamic performance degradation of the iced airfoil.

Though most of the modern aircraft today are equipped with the anti- icing or de- icing devices, due to the high installation cost and weight issues, use of these devices are restricted to the small areas of the aircraft as well as for the limited duration of time. So an efficient design of these instruments requires an understanding of the ice accretion physics. The current study thus aimed at finding out some inputs for the efficient design of such devices and also to study the ice accretion behavior for the unprotected surfaces of the aircraft for an additional safety requirement. Results found from such study will also help the pilot in pilot training on these devices and engineering evaluation of system failures due to in-flight ice accretion.

5.2 Recommendations

Due to the lack of sufficient experimental facilities in terms of flight tests and icing wind tunnel set up a numerical study is carried out to understand the ice accretion and its effects on aerodynamic performance of aircraft wing cross section under various environmental conditions. However, the following recommendations are made to extend present research further in future:

a) The prediction of ice accretion was done at a level flight (zero degree angle of attack) and then the aerodynamic performance of the iced airfoil was considered for varying angles of attack; change in the angle of attack could be taken into consideration for better understanding of the ice accretion physics.

b) A similar study could be carried out on other airfoil section as well as the whole wing section.

c) Though wind tunnels have high installations and maintenance costs, the aerodynamic performance analysis of the ice accreted airfoil could be experimentally tested in a dry-air subsonic wind tunnel for better understanding of the aerodynamic performance degradation.

d) Presently the study is undertaken where the ice accretion is de-linked with aerodynamic analysis. It is more prudent to undertake coupled icing/aerodynamic analysis using advanced tools.

REFERENCES

[1] G.T. Andreev and V.V. Bogatyrev, Investigation of Icing Effects on Aerodynamic Characteristics of Aircraft at TSAGI, 29th Congress of the International Council of the Aeronautical Sciences, Russia, September 7-12, 2014.

[2] M. K. Politovich, Aircraft Icing, National Center for Atmospheric Research, Boulder, CO, USA, 2003.

[3] S. A. Amintabar, What We Need to Know about Icing, Sources: Aircraft Loos of Control (S. R. Jacobson,2010), Appendix C, Icing Conditions, to CFR 14 Part 25, FAA, Aircraft Icing Handbook, EASA SIB, 2014.

[4] K. Mortensen, CFD Simulation of an Airfoil with Leading Edge Ice Accretion, Department of Mechanical Engineering, Technical University of Denmark, August, 2008.

[5] G. Mingione and M. Barocco, Flight in Icing Conditions Summary, October 1, 1997.

[6] A. Heinrich, R. Ross, G. Zumwalt, J. Provorse, V. Padmanabhan, J. Thompson and J. Riley, Aircraft Icing Handbook, vol. 1 of 3, pp. I 1-7, March, 1991.

[7] A. A. Shinkafi, Development of a Method to Study Aircraft Trajectory Optimization in the Presence of Icing, Department of Aerospace Engineering, Cranfield University, November, 2015.

[8] B. G. Gulick, Effects of a Simulated Ice Formation on the Aerodynamic Characteristics of an Airfoil, Wartime Report, National Advisory Committee for Aeronautics, Washington, May, 1938.

[9] D. T. Bowden, Effect of Pneumatic De-Icers and Ice Formation on Aerodynamic Characteristics of An Airfoil, National Advisory Committee for Aeronautics, Washington, February, 1956.

[10] V. H. Gray and U. H. Von Glahn, Aerodynamic Effects Caused by Icing of an Unswept NACA 65A004 Airfoil, National Advisory Committee for Aeronautics, Washington, February, 1958.

[11] P. E. Poinsatte, Heat Transfer Measurement from a NACA 0012 Airfoil In-Flight and in the NASA Lewis Icing Research Tunnel, Ohio, 1990.

[12] M. B. Bragg and M. F. Kerho, Airfoil Boundary Layer Development and Transition with Large Leading Edge Roughness, AIAA Journal, Vol. 35, No. 1, P.P 75-84, January, 1997.

[13] M. B. Bragg, Effects of Leading- Edge Ice Accretion Geometry on Airfoil Performance, AIAA-1999-3150.

[14] D. N. Anderson and J. Tsao, Evaluation and Validation of the Messinger Freezing Fraction, 41st Aerospace Sciences Meeting and Exhibit Sponsored by the American Institute of Aeronautics and Astronautics (AIAA–2003–1218), Reno, Nevada, January 6–9, 2003.

[15] A. P. Broeren and M. B. Bragg, Effect of Airfoil Geometry on Performance with Simulated Inter Cycle Ice Accretions, AIAA- 2003- 0728.

[16] C. S. Bidwell and M. Papakadis, Collection Efficiency and Ice Accretion Characteristics of Two Full- Scale and One ¼ Scale Business Jet Horizontal Tails, NASA Scientific and Technical Information Program, June 2005.

[17] T. P. Ratavasky, B. P. Barnhart and S. Lee, Current Methods for Modeling and Simulating Icing Effects on Aircraft Performance, Stability and Control, NASA Scientific and Technical Information Program, 2008.

[18] Y. Hans and J. Palacios, Airfoil- Performance- Degradation Prediction Based on Non Dimensional Icing Parameters, AIAA Journal, Volume 51, No 11, P.P 2570- 2581, November, 2013.

[19] J. Tsao and S. Lee, Evaluation of Icing Scaling on Swept NACA 0012 Airfoil Models, International Conference on Aircraft and Engine Icing and Ground Deicing, Sponsored by the SAE International, Chicago, Illinois, June 13-17, 2011.

[20] S. G. Pouryoussefi, M. Mirzaei, M. Nazemi, M. Fouladi and A. Doostmahmoudi, Experimental Study of Ice Accretion Effects on Aerodynamic Performance of an NACA 23012 Airfoil, Chinese Journal of Aeronautics, 29(3), 585-595, 2016.

[21] L. Brandrud and J. Krogenes, Aerodynamic Performance of the NREL S826 Airfoil in Icing Conditions, Department of Energy and Process Engineering, Norwegian University of Science and Technology, 11 June, 2017.

[22] I. Langmuir and K. Blodgett, Mathematical Investigation of Water Droplet Trajectories, Army Air Forces Headquarters, Air Technical Service Command; Washington, Army Air Forces Technical Report, No 5418, 1946.

[23] B. L. Messinger, Equilibrium Temperature of an Unheated Icing Surface as a Function of Air Speed, Journal of the Aeronautical Sciences, Vol. 20, No. 1, Pp. 29-42, 1953.

[24] J. Shin, B. Berkowitz, H. Chen and T. Cebeci, Prediction of Ice Shapes and Their Effect on Airfoil Performance, 29th Aerospace Sciences Meeting, AIAA, Reno, Nevada, January 7-10, 1991.

[25] D. N. Anderson, Acceptable Tolerances for Matching Icing Similarity Parameters in Scaling Applications, 29th Aerospace Sciences Meeting and Exhibit, AIAA, Reno, Nevada, January 8-11, 2001.

[26]G. Fortin and J. Laforte, A. Beisswenger, Prediction of Ice Shapes on NACA 0012 2D Airfoil, Anti- Icing Materials Laboratory, University Du Quebec A Chicoutimi, Quebec, Canada, 2003.

[27] R. A. Silveria, C. R. Maliska, D. A. Estivam and R. Mendes, Evaluation of Collection Efficiency Methods for Icing Analysis, 17th International Congress on Mechanical Engineering, Sao Paulo, Nov 10-14, 2003.

[28] C. Son, S. Oh and K. Yee, Quantitative Analysis of a Two-Dimensional Ice Accretion on Airfoils, Journal of Mechanical Science and Technology, vol 26, Issue 4, Pp. 1059–1071, April 2012.

[29] X. Zhang, J. Min and X. Wu, Model for Aircraft Icing with Consideration of Property- Variable Rime Ice, International Journal of Heat And Mass Transfer, vol. 97, pp. 185-190, June, 2016.

[30] X. Zhang, J. Min and X. Wu, Aircraft Icing Model Considering both Rime Ice Property Variability and Runback Water Effect, International Journal of Heat and Mass Transfer, vol. 104, pp. 510-516, January, 2017.

[31] W. B. Bright, A Summary of Validation Results for LEWICE 2.0, 37th Aerospace Sciences Meeting and Exhibit Sponsored by the American Institute of Aeronautics And Astronautics (AIAA–2003–1218), Reno, Nevada, January 11-14, 1999.

[32] Y. Choo, M. Vickerman, Ki D. Lee and D. S. Thompson, Geometry Modeling and Grid Generation for "Icing Effects" and "Ice Accretion" Simulations on Airfoils, 2000.

[33] H. Beaugendre, F. Morency and W.G. Habashi, Development of a Second Generation In- Flight Icing Simulation Code, Journal of Fluids Engineering, American Society Of Mechanical Engineers, 128(2), pp. 378- 387, 2006.

[34] G. Croce, W. Habashi, J. D. Munzar and G. S. Baruzzi, FENSAP-ICE: Analytical Model for Spatial and Temporal Evolution of In-Flight Icing Roughness, Journal of Aircraft 47(4):1283-1289, July 2010.

[35]M.B. Bragg, A.P. Broeren, H.E. Addy, M.G. Potapezuk, D. Guffond and E. Montreuil, Airfoil Ice Accretion Aerodynamics Simulation, 45th Aerospace Sciences Meeting and Exhibit, AIAA, Reno, Nevada, January 1-8, 2007.

[36] N. Tabatabaei, M.J. Cervantes, C. Trivedi and J. Aidanpaa, Numerical Study of Aerodynamic Characteristics of A Symmetric NACA Section With Simulated Ice Shapes, Journal of Physics: Conference Series 753, 2016.

[37] D. R. Hanson and M. P. Kinzel, "Evaluation of A Subgrid-Scale Computational Fluid Dynamics Model For Ice Roughness", Journal of Aircraft, vol. 56, No. 2, pp. 787-799, 2019.

[38] S.Ozgen and M. Cambek, Ice Accretion on Multi- Element Airfoils Using Extended Messinger Model, Journal of Heat And Mass Transfer, Volume 45, Issue 3, January, 2009.

[39] Y. S. Touloukian, P.E. Liley and S.C. Saxena, Thermo Physical Properties of Matter, Vol. 3: Thermal Conductivity, The TPRC Data Series, 1970.

[40] W. Zou, Introduction to Computational Fluid Dynamics, JASS 05, St. Petersburg.

[41] Cloud Names and Classifications, www.Metoffice.Gov.Uk.

[42] A Pilot's Guide to In flight Icing, Module- I: Before You Fly Know the Situation, Section: Weather- Cloud Formations, NASA Aircraft Icing Training.

APPENDICES

APPENDIX A

The appendix contains the MATLAB script for calculating the ice thickness and plotting the shape over the airfoil.

MATLAB Script:

```
clc
clearall
closeall
c=.5334
t=.12*c
x=0:.0005:.10668
y=5*t*[0.2969*(sqrt(x))-0.1260*x-0.3516*((x).^2)+0.2843*((x).^3)-
0.1036*((x).^4)]
plot(x/c,y/c)
radius=.0158*c
m=2
holdon
fori=1:1:length(x)-1
   X=x(i);
   Y=y(i)
   X1=x(m);
   Y1=y(m)
   m=m+1;
dels=sqrt((X-X1).^2+(Y-Y1).^2)
   f=.5
ro=919.2
theta=dels/radius
beta=cos(theta)
lwc=.001
   v=66.94
time=360
min=0
mcom=beta*lwc*v*dels
mice= f*(mcom+min)
   h=((mice*time)/(ro*dels))
end
xp=radius
yp=0
th=pi/4.6:pi/400:pi
a=(radius+h)*cos(th)+xp
b=(radius+h)*sin(th)+yp
plot(a/c,b/c,'r')
gridon
holdon
c1=.5334
t1=.12*c
x1=0:.0005:.10668
y1=-5*t1*[0.2969*(sqrt(x1))-0.1260*x1-0.3516*((x1).^2)+0.2843*((x1).^3)-
0.1036*((x1).^4)]
plot(x1/c1,y1/c1)
```

```
radius1=.0158*c1
m1=2
holdon
for i1=1:1:length(x1)-1
   X1=x1(i1);
   Y1=y1(i1)
   X11=x1(m1);
   Y11=y1(m1)
   m1=m1+1;
   dels1=sqrt((X1-X11).^2+(Y1-Y11).^2)
   f1=.5
   ro1=919.2
   theta1=dels1/radius1
   beta1=cos(theta1)
   lwc1=.001
   v1=66.94
   time1=360
min1=0
   mcom1=beta1*lwc1*v1*dels1
mice1= f1*(mcom1+min1)
   h1=((mice1*time1)/(ro1*dels1))
end

xp1=radius1
yp1=0
th1=pi:pi/400:(3*pi)/1.68
a1=(radius1+h1)*cos(th1)+xp1
b1=(radius1+h1)*sin(th1)+yp1
plot(a1/c1,b1/c1,'r')
gridon
title('ice profile f=.5,t=360s')
xlabel('x/c')
ylabel('y/c')
```

APPENDIX B

Parameters and Calculated ice thickness at the stagnation point for different cases:

Case I: (Re= 6×10^6)

Serial	Freezing fraction, f	Time of accretion, s	Ice thickness, m
a	3	600	.0193
b	.5	300	.01605
c	.7	120	.0089
d	.7	600	.0449
e	1	120	.0128
f	1	300	.0321
g	1	600	.0642

Case II: (Re= 6×10^6)

Serial	Freezing fraction, f	Time of accretion, s	Ice thickness, m
a	3	700	.0385
b	.5	500	.0275
c	.7	300	.035
d	.7	700	.0898
e	1	80	.0146
f	1	300	.0550
g	1	700	.1282

Case III: (Re= 6×10^6)

Serial	Freezing fraction, f	Time of accretion, s	Ice thickness, m
a	3	500	.0307
b	.5	200	.0204
c	.7	200	.0286
d	.7	500	.0715
e	1	50	.0102
f	1	200	.0409
g	1	500	.1022

Reynolds Number Variation:

Case IV: (Re= 5×10^6)

Serial	Freezing fraction, f	Time of accretion, s	Ice thickness, m
a	3	700	.0320
b	.5	500	.0381
c	.7	300	.0320
d	.7	700	.0747
e	1	80	.0122
f	1	300	.0457
g	1	700	.1067

Case V: (Re= 8×10^6)

Serial	Freezing fraction, f	Time of accretion, s	Ice thickness, m
a	3	700	.0361
b	.5	500	.0429
c	.7	300	.0361
d	.7	700	.0842
e	1	80	.0137
f	1	300	.0515
g	1	700	.1202

Case VI: (Re= 15×10^6)

Serial	Freezing fraction, f	Time of accretion, s	Ice thickness, m
a	3	700	.0483
b	.5	500	.0575
c	.7	300	.0483
d	.7	700	.0563
e	1	80	.0184
f	1	300	.0691
g	1	700	.1611

APPENDIX C

Standard Atmosphere, SI Units:

Altitude		Temperature	Pressure	Density
h_G, m	h, m	T, K	p, N/m^2	ρ, kg/m^3
2,000	1,999	275.16	7.9501 + 4	1.0066 + 0
2,100	2,099	274.51	7.8520	9.9649 − 1
2,200	2,199	273.86	7.7548	9.8649
2,300	2,299	273.22	7.6586	9.7657
2,400	2,399	272.57	7.5634	9.6673
2,500	2,499	271.92	7.4692	9.5696
2,600	2,599	271.27	7.3759	9.4727
2,700	2,699	270.62	7.2835	9.3765
2,800	2,799	269.97	7.1921	9.2811
2,900	2,899	269.32	7.1016	9.1865
3,000	2,999	268.67	7.0121 + 4	9.0926 − 1
3,100	3,098	268.02	6.9235	8.9994
3,200	3,198	267.37	6.8357	8.9070
3,300	3,298	266.72	6.7489	8.8153
3,400	3,398	266.07	6.6630	8.7243
3,500	3,498	265.42	6.5780	8.6341
3,600	3,598	264.77	6.4939	8.5445
3,700	3,698	264.12	6.4106	8.4557
3,800	3,798	263.47	6.3282	8.3676
3,900	3,898	262.83	6.2467	8.2802
4,000	3,997	262.18	6.1660 + 4	8.1935 − 1
4,100	4,097	261.53	6.0862	8.1075
4,200	4,197	260.88	6.0072	8.0222
4,300	4,297	260.23	5.9290	7.9376
4,400	4,397	259.58	5.8517	7.8536
4,500	4,497	258.93	5.7752	7.7704
4,600	4,597	258.28	5.6995	7.6878
4,700	4,697	257.63	5.6247	7.6059
4,800	4,796	256.98	5.5506	7.5247
4,900	4,896	256.33	5.4773	7.4442
5,000	4,996	255.69	5.4048 + 4	7.3643 − 1
5,100	5,096	255.04	5.3331	7.2851
5,200	5,196	254.39	5.2621	7.2065
5,300	5,296	253.74	5.1920	7.1286
5,400	5,395	253.09	5.1226	7.0513
5,500	5,495	252.44	5.0539	6.9747
5,600	5,595	251.79	4.9860	6.8987
5,700	5,695	251.14	4.9188	6.8234
5,800	5,795	250.49	4.8524	6.7486
5,900	5,895	249.85	4.7867	6.6746
6,000	5,994	249.20	4.7217 + 4	6.6011 − 1
6,100	6,094	248.55	4.6575	6.5283
6,200	6,194	247.90	4.5939	6.4561
6,300	6,294	247.25	4.5311	6.3845
6,400	6,394	246.60	4.4690	6.3135
6,500	6,493	245.95	4.4075	6.2431

Altitude		Temperature	Pressure	Density
h_G, m	h, m	T, K	p, N/m^2	ρ, kg/m^3
6,600	6,593	245.30	4.3468	6.1733
6,700	6,693	244.66	4.2867	6.1041
6,800	6,793	244.01	4.2273	6.0356
6,900	6,893	243.36	4.1686	5.9676
7,000	6,992	242.71	4.1105 + 4	5.9002 − 1
7,100	7,092	242.06	4.0531	5.8334
7,200	7,192	241.41	3.9963	5.7671
7,300	7,292	240.76	3.9402	5.7015
7,400	7,391	240.12	3.8848	5.6364
7,500	7,491	239.47	3.8299	5.5719
7,600	7,591	238.82	3.7757	5.5080
7,700	7,691	238.17	3.7222	5.4446
7,800	7,790	237.52	3.6692	5.3818
7,900	7,890	236.87	3.6169	5.3195
8,000	7,990	236.23	3.5651 + 4	5.2578 − 1
8,100	8,090	235.58	3.5140	5.1967
8,200	8,189	234.93	3.4635	5.1361
8,300	8,289	234.28	3.4135	5.0760
8,400	8,389	233.63	3.3642	5.0165
8,500	8,489	232.98	3.3154	4.9575
8,600	8,588	232.34	3.2672	4.8991
8,700	8,688	231.69	3.2196	4.8412
8,800	8,788	231.04	3.1725	4.7838
8,900	8,888	230.39	3.1260	4.7269
9,000	8,987	229.74	3.0800 + 4	4.6706 − 1
9,100	9,087	229.09	3.0346	4.6148
9,200	9,187	228.45	2.9898	4.5595
9,300	9,286	227.80	2.9455	4.5047
9,400	9,386	227.15	2.9017	4.4504
9,500	9,486	226.50	2.8584	4.3966
9,600	9,586	225.85	2.8157	4.3433
9,700	9,685	225.21	2.7735	4.2905
9,800	9,785	224.56	2.7318	4.2382
9,900	9,885	223.91	2.6906	4.1864
10,000	9,984	223.26	2.6500 + 4	4.1351 − 1
10,100	10,084	222.61	2.6098	4.0842
10,200	10,184	221.97	2.5701	4.0339
10,300	10,283	221.32	2.5309	3.9840
10,400	10,383	220.67	2.4922	3.9346
10,500	10,483	220.02	2.4540	3.8857
10,600	10,582	219.37	2.4163	3.8372
10,700	10,682	218.73	2.3790	3.7892
10,800	10,782	218.08	2.3422	3.7417
10,900	10,881	217.43	2.3059	3.6946
11,000	10,981	216.78	2.2700 + 4	3.6480 − 1
11,100	11,081	216.66	2.2346	3.5932

Source: J. D. Anderson, Introduction to Flight, 3rd Edition, page: 561-562

Approximate heights and limits of the clouds at different regions:

Etages	*Polar Regions*	*Temperate Regions*	*Tropical Regions*
High	3–8 km (10 000–25 000 ft)	5–13 km (16 500–45 000 ft)	6–18 km (20 000–60 000 ft)
Middle	2–4 km (6 500–13 000 ft)	2–7 km (6 500–23 000 ft)	2–8 km (6 500–25 000 ft)
Low	From the Earth's surface to 2 km (6 500 ft)	From the Earth's surface to 2 km (6 500 ft)	From the Earth's surface to 2 km (6 500 ft)

Source: International Cloud Atlas, Volume I, Page: 15, Revised Edition 1975, Manual of the Observation of Clouds and other Meteors, World Meteorological Organization (WMO).